

ComEMS4Build: Comfort-Oriented Energy Management System for Residential Buildings using Hydrogen for Seasonal Storage

Jovana Kovačević*, Felix Langner, Erfan Tajalli-Ardekani, Marvin Dorn, Simon Waczowicz, Ralf Mikut, Jörg Matthes, Hüseyin K. Çakmak, Veit Hagenmeyer

Karlsruhe Institute of Technology, Institute for Automation and Applied Informatics, Eggenstein-Leopoldshafen, Germany

Abstract

Integrating flexible loads and storage systems into the residential sector contributes to the alignment of volatile renewable generation with demand. Besides batteries serving as a short-term storage solution, residential buildings can benefit from a Hydrogen (H_2) storage system, allowing seasonal shifting of renewable energy. However, as the initial costs of H_2 systems are high, coupling a Fuel Cell (FC) with a Heat Pump (HP) can contribute to the size reduction of the H_2 system. The present study develops a Comfort-Oriented Energy Management System for Residential Buildings (ComEMS4Build) comprising Photovoltaics (PV), Battery Energy Storage System (BESS), and H_2 storage, where FC and HP are envisioned as complementary technologies. The fuzzy-logic-based ComEMS4Build is designed and evaluated over a period of 12 weeks in winter for a family household building in Germany using a semi-synthetic modeling approach. The Rule-Based Control (RBC), which serves as a lower benchmark, is a scheduler designed to require minimal inputs for operation. The Model Predictive Control (MPC) is intended as a cost-optimal benchmark with an ideal forecast. The results show that ComEMS4Build, similar to MPC, does not violate the thermal comfort of occupants in 10 out of 12 weeks, while RBC has a slightly higher median discomfort of 0.68 Kh. The ComEMS4Build increases the weekly electricity costs by 12.06 € compared to MPC, while RBC increases the weekly costs by 30.14 €. The ComEMS4Build improves the Hybrid Energy Storage System (HESS) utilization and energy exchange with the main grid compared to the RBC. However, when it comes to the FC operation, the RBC has an advantage, as it reduces the toggling counts by 3.48% and working hours by 7.59% compared to MPC. The ComEMS4Build works on lower FC load and higher FC electrical efficiencies, increasing working hours by 48.44% and toggling 6.09%, compared to MPC. However, as RBC does not contain inputs about H_2 usage, it empties the H_2 storage much earlier than the other two energy management systems. The proposed ComEMS4Build offers a model- and forecast-free alternative to MPC that improves occupant comfort and HESS utilization over a simple RBC, requiring minimal additional input data and making it suitable for real-world deployment.

Keywords: Buildings, Comfort-oriented control, Demand response, Energy management system, Fuzzy logic, Hydrogen, Model predictive control

1. Introduction

Microgrids at district and residential levels, as well as buildings with Distributed Energy Resources (DER), are gaining attention as a solution to relieve the grid by reducing the need for energy imports [1, 2]. Furthermore, residential buildings with DER are providing residents with flexibility of energy usage with partial or full autonomy. Focusing on decarbonization, the integration of Renewable Energy Source (RES), such as Photovoltaics (PV) and Wind Turbines (WT), in the residential sector poses a challenge in balancing the volatile production of RES with residential energy demand [3]. To introduce flexibility into the residential buildings from an electrical perspective, it is necessary to integrate storage systems for capturing energy produced during periods when it is not being utilized

*Corresponding author

Email address: jovana.kovacevic@kit.edu (Jovana Kovačević)

Nomenclature

Acronyms

BESS	Battery Energy Storage System
COP	Coefficient of Performance
DER	Distributed Energy Resources
DHW	Domestic Hot Water
EDF	Empirical Distribution Function
EL	Electrolyzer
EMS	Energy Management System
FC	Fuel Cell
FLC	Fuzzy Logic Controller
HESS	Hybrid Energy Storage System
HP	Heat Pump
LOH	Level of Hydrogen
MPC	Model Predictive Control
PV	Photovoltaics
RBC	Rule-Based Control
RES	Renewable Energy Source
SH	Space Heating
SOC	State of Charge
TBM	Thermal Building Mass

Parameters

η	Efficiency in %
σ	Costs in €, €/h or €/Wh
ζ	Security factor
C	Heat capacity in J/K
f	Heat flux factor
g	Heat gain factor in m ²
H	Number of time steps in the horizon
k	Time step
M	Number of time steps in a 7 days week
N	Total number of time steps
R	Thermal resistance in K/W
t_s	Sample time in s
LHV	Lower heating value in J/kg

Subscripts

air	Indoor air
-----	------------

amb	Ambient air
buy	Purchase price
B	Battery
ch	Charging
conv	Convective
dm	Demand
d	Discharging
el	Electrical
hr	Heat recovery
h	Heating
in	Investment
l	Heat loss
om	Operation and maintenance
sys	System
s	Solar
th	Thermal
we	Week
w	Wall

Variables

α	ComEMS4Build control output
χ	State factor
ΔLOH	Permissible daily amount of H ₂ in kWh
\dot{n}	Molar flow in mol/s
\dot{Q}	Heat flow in W
\dot{q}	Radiation in W/m ²
\hat{p}	Empirical distribution function
E	Energy in kWh
P	Power in W
p	Price in €/kWh
s	Binary variable
T	Temperature in °C
u	MPC Control input
x	State
y	MPC control output
T	Toggling counts
WH	Working hours

directly [4]. For this, the BESS contributes to the system's flexibility on a daily and up to weekly basis, by storing renewable energy for later consumption. However, the issue of aligning power generation and consumption does not only occur daily but also between seasons, when BESS lacks the capability to capture this discrepancy due to their low energy density and high self-discharge rate [5]. The H₂ storage system, as a long-term seasonal storage solution, overcomes this challenge, as it exhibits a low leakage rate and high energy density, storing the energy in the form of H₂ during the sunny summer months. The H₂ can then be utilized to generate power during the winter period, when demand is at its peak. The utilization of H₂ system solutions within residential buildings is not considered to be the optimal solution due to the high investment costs and low efficiencies associated with it. However, it should be noted that there do not exist many other alternative solutions for long-term energy storage [6]. Although they are not yet economically viable, H₂ systems play an integral role in resilient energy systems, achieving building energy autonomy and operating even during power grid outages [7]. Moreover, as buildings have a significant impact on the transition to sustainability, integration of H₂ systems combined with RES can reduce greenhouse gas emissions, as addressed in [8]. Capturing waste heat from the Fuel Cell (FC) contributes to enhancing the system's efficiency by reducing the demand for Heat Pump (HP) utilization. When considering FC in the Combined Heat and Power (CHP) mode, they can achieve overall efficiencies of 90% [9, 10]. Furthermore, technological advancements have been shown to extend the operational lifespan of H₂ systems [9], improving their economic viability. In addition, it is anticipated that economies of scale will result in a reduction of the investment costs associated with H₂ systems [2, 11].

The flexibility can be further leveraged by exploiting the heating systems of residential buildings, particularly if they are electrified. For this, the Thermal Building Mass (TBM) can be exploited as thermal storage, especially when heating bodies have high inertia, such as underfloor heating systems. Integrating a hybrid storage system that includes BESS and H₂ storage, as well as thermal storage for Domestic Hot Water (DHW) and TBM, enhances the alignment of renewable generation and residential demand, thereby improving the security of the building's power supply [12].

In residential buildings with versatile DER, the Energy Management System (EMS) is a critical component, as it impacts the overall system's efficiency, thereby enhancing its commercial viability [13]. According to [14], a notable research gap has been identified in the field of advanced control strategies for H₂-based residential buildings. Thus, the present study develops the EMS scheduler, a Comfort-Oriented Energy Management System for Residential Buildings (ComEMS4Build) which couples FC and HP. Besides the management of the HESS, i.e., BESS and H₂ storage, the novel algorithm considers the TBM as additional auxiliary storage while considering the thermal comfort of the occupants in the building. Introducing the TBM in the scheduling algorithm contributes further to demand-side response and flexible heating load shifting. The developed forecast- and model-free ComEMS4Build EMS is benchmarked with Rule-Based Control (RBC) and Model Predictive Control (MPC), where all three have different levels of knowledge about the building and DER state.

1.1. Related work

HESSs play a crucial role in improving self-sufficiency and minimizing operational costs for both large-scale energy systems, as noted by Yang et al. [15], and residential building applications, as discussed by Go et al. [16]. Among the multiple existing operational scenarios of HESS, it has been widely proven that the BESS as a short-term and H₂ as a long-term storage system are the most common combination in energy systems with high shares of RESs [17, 18]. Çiçek et al. [19] implement a Mixed-Integer Linear Programming (MILP) approach to ensure the economic and uninterrupted operation of H₂-integrated green buildings. By analyzing a building with 40 apartments equipped with H₂-powered boilers, H₂ electric vehicles, and FC, it is concluded that the resilience of the building and continuous operation are maintained during H₂ and electricity power outages. Moreover, the integration of RESs and FC results in a 29% reduction in operational costs. Utilizing the electrical demands of an office building, Li et al. [20] propose a hybrid energy system comprising a BESS, FC, and Electrolyzer (EL). The developed game-theory-based power management system extends the operational lifespan of the FC and reduces power output fluctuations.

Go et al. [16] investigate the role of HESS consisting of BESS and H₂ in maximizing the self-sufficiency of residential building energy supplying systems. The role of the H₂ storage system in the HESS highlights not only compensating for self-discharge BESS losses but also minimizing carbon dioxide (CO₂) emissions. The heat generated during the FC operation can be recovered and reused to satisfy the building's Space Heating (SH) and DHW demands. Ou et al. [21] develop and validate an optimal EMS for a safe and efficient operation of a HESS, including FC, BESS, and a thermal storage. They highlight that the heat recovery from the FC operation can increase the overall system efficiency by 20%. The heat recovery potential of using a residential-scale (1 kW) FC in conjunction with an

underfloor heating system is investigated by Gandiglio et al. [22]. They illustrate that the usage of heat recovery in the proposed energy system increases the overall FC system efficiency by more than 75%. Oh et al. [23] evaluate the feasibility of introducing a FC-based energy system in a residential apartment using a thermo-economic approach. The combined generation of heat and power by the proposed system results in a 20% operational cost savings compared to the bill for running conventional systems.

EMSs employ a combination of strategies and operating scenarios to improve the efficiency and performance of DER in residential buildings [24]. The most common and widely used EMS techniques are MPC [12], Fuzzy Logic Controller (FLC) [25], RBC [26], and Reinforcement Learning (RL) [27]. However, these techniques have strengths and weaknesses [13], and their applications depend on specific use cases. MPC offers a powerful control strategy and is often used to obtain optimal EMS schedulers. However, the model-dependency and relatively high computational costs of such a technique are limiting [28, 29]. Wang et al. [12] develop a dual-layer MPC and apply it to off-grid operation of residential buildings in northern China. They conclude that the feasibility of the optimized economic operations of the HESS, which comprises both BESS and H₂ storage units, is demonstrated. In contrast to MPC, FLC and RL do not depend on the system model, have low and affordable computational costs, but optimal performance is not always guaranteed [13]. Soft-computing capabilities, managing complex systems, and handling uncertainties make FLC a proper candidate to govern the building's EMS. Maroufi et al. [30] explore the FLC role in the power distribution of a HESS between a flywheel and a BESS. They showcase the dynamic implementation of FLC for optimal BESS performance through minimization of the battery's ramp rate and ensure efficient flywheel's operation through the flywheel's State of Charge (SOC) corrections. Boynuegri et al. [31] study the load shifting potentials of a home EMS using FLC. The target is to reduce the H₂ consumption of the off-grid house, which is being supplied by renewable sources (PV and WT). They conclude that the FLC-integrated EMS is capable of reducing the H₂ consumption of the FC by 7.03% and increasing the annual FC efficiency by 4.6% compared to a conventional EMS, where the FC is operated directly after the insufficiency of RES power generation. However, the flexibility capabilities of BESS and the waste heat recovery potentials of FC are not investigated. Considering a single-family house in Croatia, Šanić et al. [26] study the performance of a stand-alone micro-trigeneration system, i.e., combined cooling, heating, and power, consisting of a HESS. With a rule-based EMS they can cover 80% of the thermal loads by utilizing the waste heat of FC and HP while working in cooling mode during the summer in a Mediterranean climate. However, they do not explore the thermal flexibility of the building. Vivas et al. [25] develop an EMS that integrates FLC and apply it to a residential-type DC building including HESS. However, they use the expected demand profiles for thermal and electrical consumption, with no thermal flexibility of the building being explored. The potential of the fuzzy logic-based EMS in reducing grid imports (to 83 kWh) compared to previously developed hysteresis-based (430 kWh) and specific MPC-based (159 kWh) EMSs is concluded. Moreover, the proposed EMS has reduced the degradation of the BESS and FC stack by 60% compared to the MPC-based strategies.

1.2. Contribution of the present paper

The FC and HP were initially considered as competing technologies [2, 32]. However, in recent years, they have gained popularity as complementary technologies, where, for example, Andrade et al. [33] demonstrate that integrating the HP and FC in the European climate achieves the reduction of the FC size for at least 40% (northern Europe), simultaneously decreasing the initial investment costs. In contrast, the HP can contribute to energy savings of 20%. To the best of the authors' knowledge, there is no detailed evaluation of exploiting the flexibility in a hybrid setup, where FC reduces the dependence of the building on the main grid via H₂ utilization, and HP can contribute to load shifting, utilizing the TBM as storage in addition to HESS. The main contributions of the present paper are as follows:

- Introduction of an Energy Management System (EMS) for a residential building configuration that integrates a Fuel Cell (FC) and a Heat Pump (HP) operating in heating mode. The building is complemented by a Photovoltaics (PV), a Battery Energy Storage System (BESS), and a Domestic Hot Water (DHW) storage.
- Design of a forecast-free and model-free demand-response EMS that accounts for occupant thermal comfort while exploiting the TBM as an additional storage medium.
- Evaluation of heat recovery performance within the proposed building setup under varying FC efficiencies as reported in the literature.

- Benchmarking of the proposed ComEMS4Build EMS against a cost-optimal MPC, requiring forecast models, and RBC, designed to operate with minimal inputs.

Besides the inputs about the system's state and day-ahead electricity price signal, implemented in RBC, the ComEMS4Build requires further future temperature constraints, current solar radiation, permissible daily H₂ usage, and the former state of the FC to exploit further flexibility of HESS, TBM and thermal storage. Moreover, in addition to these inputs, the MPC requires forecasting models and profiles, such as weather data, demand, and building behavior forecasts.

1.3. Structure of the present paper

The remainder of the paper is structured as follows: Section 2 is divided into two subsections: Subsection 2.1 describes the models used within the building, and Subsection 2.2 gives an overview of control algorithms. Section 3 provides the data, parameters, simulation setup, and evaluation metrics. The results are presented in Section 4 and discussed in Section 5. Finally, the paper is concluded in Section 6 where the outlook for future work is further discussed.

2. Methodology

Figure 1 illustrates the considered building setup, including all components and their corresponding electricity, heat, and H₂ flows. The residential building represents a typical 4-person household. The HESS consists of a short-term BESS storage and a long-term H₂ storage. The SOC indicates the level of electrical energy stored in BESS, while the fill level of H₂ storage is indicated by the Level of Hydrogen (LOH). The state of the main grid is represented with dynamic electricity pricing, and the PV is integrated as a distributed energy source. Besides the DHW storage, the TBM contributes to flexibility as an auxiliary thermal storage. The latter two are depicted in Figure 1 with a red background indicating the thermal storage system. The three developed scheduling algorithms include the MPC as an optimal-based scheduler, which is used in this case with ideal forecasting. MPC is envisioned as the benchmark controller, with the highest number of inputs. Secondly, the ComEMS4Build has a lower number of inputs than the MPC. It does not require forecasting models and profiles like the MPC, but still requires some additional inputs, described in detail in Section 2.2.2. We construct the third scheduler, a simple RBC, as the lowest benchmark. It is derived from ComEMS4Build rules and further simplified. The RBC is designed to require minimal inputs for operating a building's DER.

2.1. Models

This section describes the models used for evaluating the scenarios. Sections 2.1.1 and 2.1.2 describe the PV generation and BESS, respectively. The H₂ system composed of the FC and H₂ storage is described in Section 2.1.3. Sections 2.1.4 and 2.1.5 follow with the description of the HP's energy conversion and DHW storage system. Finally, to exploit the thermal building flexibility, the building model is described in Section 2.1.6.

2.1.1. Photovoltaics (PV)

The PV generation defined in existing literature [34] is outlined with the Equation (1). It is subject to the number of modules n_{module} , the area of each module a_{module} in m² and the incident solar radiation falling on the tilted module $G[k]$ in the time step k calculated in W/m². The incident solar radiation $G[k]$ is calculated based on global radiation \dot{q}_s , diffuse solar radiation, and tilted angle [35]. The $NOCT$ represents the nominal operating cell temperature, T_{amb} is the ambient air temperature, and T_{STC} is the temperature under the standard testing conditions. All latter three are defined in °C. The term $(NOCT - 20^\circ\text{C})/800\text{W/m}^2$ represents the overall heat loss coefficient in °C/(W/m²) [36]. Besides that the power generated $P_{\text{PV}}[k]$ is determined by following efficiencies η_{STC} - electrical efficiency of the PV module at standard testing conditions, $\eta_{\text{L\&T}}$ - combined energy reduction due to the inverter and the maximum power point tracking controller, and temperature coefficient η_T in 1/°C of PV generation:

$$P_{\text{PV}}[k] = n_{\text{module}} \cdot a_{\text{module}} \cdot G[k] \cdot \eta_{\text{STC}} \cdot \eta_{\text{L\&T}} \cdot \left[1 - (\eta_T \cdot (T_{\text{amb}}[k] + \frac{NOCT - 20^\circ\text{C}}{800\text{W/m}^2} \cdot G[k] - T_{\text{STC}})) \right] \quad (1)$$

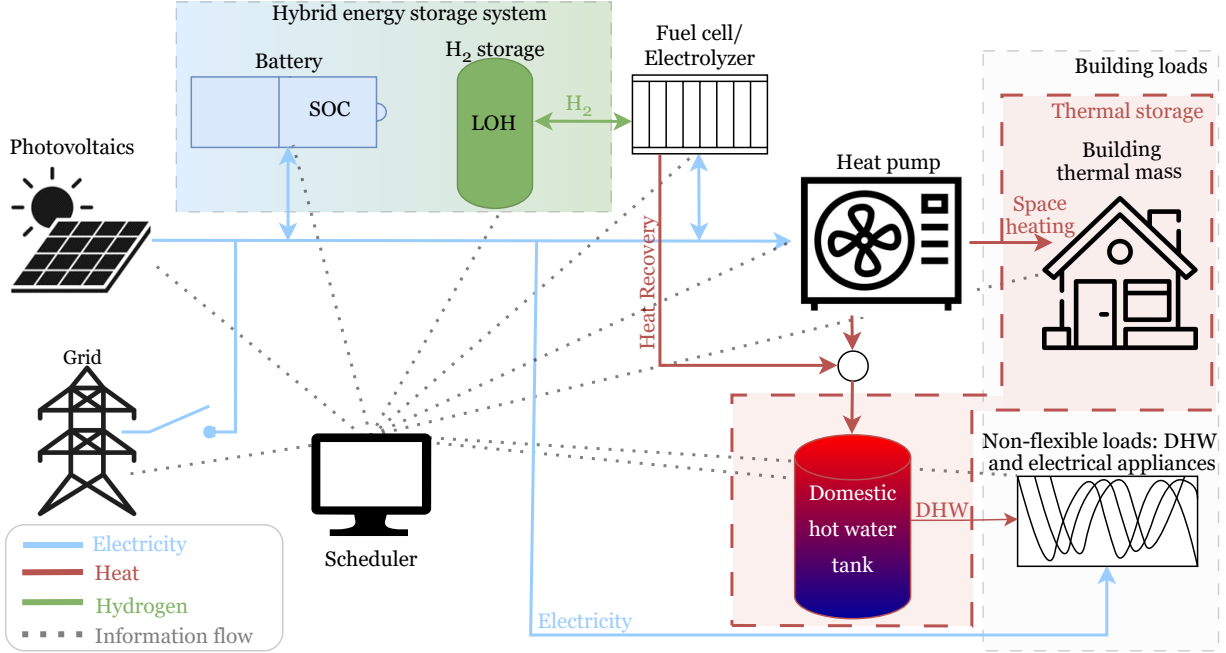


Figure 1: The residential building with HESS, PV, HP, DHW storage and TBM as an additional thermal storage.

2.1.2. Battery Energy Storage System (BESS)

The $SOC[k]$ at time step k , Equation (2), as derived from the existing literature [37], depends on the previous state $SOC[k - 1]$, the charging and discharging power $P_{ch}[k]$ and $P_d[k]$, respectively, and the efficiency of the charging and discharging processes η_{ch} and η_d , respectively, and the maximum capacity $E_{B,max}$. The parameter t_s indicates sample time in hours:

$$SOC[k] = SOC[k - 1] + (\eta_{ch} \cdot P_{ch}[k] \cdot t_s - \frac{P_d[k]}{\eta_d} \cdot t_s) / E_{B,max} \quad (2)$$

However, the effect of BESS self-discharge has not been taken into account, as the BESS is charged and discharged daily. The BESS is constrained by Equations (3) and (4). The binary variables $s_{ch}[k]$ and $s_d[k]$, defined in Equations (5) and (6), are employed to restrict charging and discharging concurrently, i.e., either the BESS is charging $s_{ch}[k] = 1$ and $s_d[k] = 0$, discharging $s_{ch}[k] = 0$ and $s_d[k] = 1$ or not used at all $s_{ch}[k] = 0$ and $s_d[k] = 0$:

$$SOC_{min} \leq SOC[k] \leq SOC_{max} \quad (3)$$

$$s_c[k] \cdot P_{c,min} \leq P_c[k] \leq s_c[k] \cdot P_{c,max} \quad (4)$$

$$s_c[k] \in \{0, 1\}; \quad \forall c \in \{ch, d\} \quad (5)$$

$$s_{ch}[k] + s_d[k] \in \{0, 1\} \quad (6)$$

2.1.3. Hydrogen (H_2) system

Green H_2 , ideally generated in summer utilizing EL when RES generation exceeds the demand, is stored in the H_2 storage. When required, the H_2 is converted back into electricity by the FC. As the FC generates a byproduct in the form of heat, it is employed as a cogeneration utility, wherein heat is recovered and utilized for the DHW demand. The H_2 system is modeled in accordance with the approaches frequently employed in the existing literature [3, 38, 39]. The molar H_2 flow consumed by FC \dot{n}_{FC} , calculated in mol/s and presented in Equation (7), is a function of the FC's power generation $P_{el,FC}$. The electrical efficiency $\eta_{el,FC}[k]$ is then calculated based on Faraday's law using the lower heating value of H_2 LHV for each time step k , as shown in Equation (8):

$$\dot{n}_{FC} = f(P_{el,FC}) \quad (7)$$

$$\eta_{el,FC}[k] = \frac{P_{el,FC}[k]}{\dot{n}_{FC}[k] \cdot LHV} \quad (8)$$

Analogously to the BESS, the LOH in the storage is measured in terms of the energy content of H_2 in the storage, as indicated by Equation (9). It depends on the previous state and the difference between the H_2 consumed at the time step k :

$$LOH[k] = LOH[k-1] - \dot{n}_{FC}[k] \cdot LHV \cdot t_s / E_{H_2,max} \quad (9)$$

The ideal gas law is used as the H_2 can be stored at lower pressures, such as 13.8-30 bar, [3, 40]. Moreover, when producing H_2 during the summer, there would be no additional losses due to compression, as EL is capable of compressing H_2 at the above-mentioned pressure levels [40]. The system is constrained by:

$$LOH_{min} \leq LOH[k] \leq LOH_{max} \quad (10)$$

$$P_{el,FC,min} \cdot s_{FC}[k] \leq P_{el,FC}[k] \leq \zeta \cdot P_{el,FC,max} \cdot s_{FC}[k] \quad (11)$$

$$(12)$$

where H_2 storage is restricted by minimal and maximal LOH_{min} and LOH_{max} calculated in kWh. The FC is constrained by corresponding minimal and maximal power $P_{el,FC,min}$ and $P_{el,FC,max}$. The factor ζ is a safety factor for degradation.

The calculation of the heat generated by FC can be performed, as outlined in [21], by utilizing the known molar H_2 flow consumed, $\dot{n}_{FC}[k]$ in conjunction with the established thermal efficiency $\eta_{th,FC}$. For this, the thermal efficiency $\eta_{th,FC}$ is obtained by subtracting the electrical efficiency $\eta_{el,FC}$ from the system's efficiency of the FC $\eta_{sys,FC}$:

$$\dot{Q}_{hr,FC}[k] = \dot{n}_{FC}[k] \cdot \eta_{th,FC}[k] \cdot LHV \quad (13)$$

$$\eta_{th,FC}[k] = \eta_{sys,FC}[k] - \eta_{el,FC}[k] \quad (14)$$

2.1.4. Heat Pump (HP) model

The HP model is employed to transform electrical power $P_{el,HP}$ into heat flux \dot{Q}_h , which is subsequently utilized for SH or DHW. The HPs' Coefficient of Performance (COP) and maximal electricity power intake $P_{el,HP,max}$ are contingent on the ambient air temperature T_{amb} and supply water temperature, which is either 55 °C for SH or 45 °C for DHW. The modulation factor η_{HP} dictates the electrical power intake of the HP and is controlled by EMS controllers. It is constrained to be either between 0.2 and 1 or the HP is turned off:

$$\dot{Q}_h[k] = COP[k] \cdot P_{el,HP}[k], \quad COP[k] = COP(T_{amb}[k], T_{supply}[k]) \quad (15)$$

$$P_{el,HP}[k] = \eta_{HP}[k] P_{el,max}[k], \quad \eta_{HP} \in \{0, [0.2, 1]\} \quad (16)$$

The utilization of the heat flux for DHW or SH is determined by the EMS and described by Equations (17) - (20). The binary operator s_{SH} is set to 1 when heating is employed for SH, and s_{DHW} is set to 1 when HP is employed for DHW, without permitting both to be utilized synchronously:

$$s_{SH}[k], s_{DHW}[k] \in \{0, 1\} \quad (17)$$

$$s_{SH}[k] + s_{DHW}[k] \in \{0, 1\} \quad (18)$$

$$\dot{Q}_{h,SH}[k] = s_{SH}[k] \dot{Q}_h[k] \quad (19)$$

$$\dot{Q}_{h,DHW}[k] = s_{DHW}[k] \dot{Q}_h[k] \quad (20)$$

2.1.5. Domestic Hot Water (DHW) storage

The DHW storage is modeled using the energy difference equation (Equation (21)). It is designed to maintain the constant temperature $T_{\text{DHW}} = \text{const.}$, while the usable volume of the storage V_{DHW} in m^3 is subject to variation. The ΔT_{DHW} describes the difference between the desired water T_{DHW} and the tap water temperature. The total heat flow \dot{Q}_{DHW} entering the system is the sum of the heat flows from HP and the heat recovered from FC (Equation (22)). The parameters $\rho_{\text{H}_2\text{O}}$ and $c_{\text{H}_2\text{O}}$ are the density and specific heat capacity of the water, respectively. The DHW demand is denoted by $\dot{Q}_{\text{dm,DHW}}$ and the standing losses by $\dot{Q}_{\text{l,DHW}}$. All heat flows are calculated in W. The sole constraint employed in this model concerns the minimum and maximum usable volumes of the storage, denoted by $V_{\text{DHW,min}}$ and $V_{\text{DHW,max}}$, respectively. For more information about the thermal storage model, we refer to [41]:

$$V_{\text{DHW}}[k] = V_{\text{DHW}}[k-1] + \frac{\dot{Q}_{\text{DHW}}[k] - \dot{Q}_{\text{dm,DHW}}[k] - \dot{Q}_{\text{l,DHW}}}{\Delta T_{\text{DHW}} \cdot \rho_{\text{H}_2\text{O}} \cdot c_{\text{H}_2\text{O}}} \cdot t_s \quad (21)$$

$$\dot{Q}_{\text{DHW}}[k] = \dot{Q}_{\text{h,DHW}}[k] + \dot{Q}_{\text{hr,FC}}[k] \quad (22)$$

$$V_{\text{DHW,min}} \leq V_{\text{DHW}}[k] \leq V_{\text{DHW,max}} \quad (23)$$

2.1.6. Building model

The thermal dynamics of the building are represented as a reduced-order building model. The 4R3C model is derived from [42] and comprises Equation (24), which describes the indoor air dynamics, denoted by subscript air, and Equations (25) and (26) describing the dynamics of internal and external temperatures of the building envelope, denoted with subscripts w,in and w,out, respectively. The thermal resistors, denoted by R_s in K/W , indicate the insulation properties of the building, whereas the thermal capacitances C_s in J/K are associated with heat storage. The temperature nodes T_{air} , $T_{\text{w,in}}$, and $T_{\text{w,out}}$ measured in K, are the indoor air, internal wall, and external wall temperatures, respectively. Weather-related parameters that affect the building dynamics are ambient air temperature T_{amb} and solar radiation \dot{q}_s , while g_s represents the solar heat gain factor. The $\dot{Q}_{\text{h,SH}}$ denotes the heat flux emitted by the HP, the f_{conv} is the convective share of HP's heat flux and $T_{\text{amb,eq}}$ is the equivalent outdoor temperature at the exterior surfaces after accounting for solar radiation:

$$C_{\text{air}} \frac{dT_{\text{air}}}{dt} = \frac{T_{\text{w,in}} - T_{\text{air}}}{R_{\text{w,air}}} + \frac{T_{\text{amb}} - T_{\text{air}}}{R_{\text{air,amb}}} + g_s \dot{q}_s + f_{\text{conv}} \dot{Q}_{\text{h,SH}} \quad (24)$$

$$C_{\text{w}} \frac{dT_{\text{w,in}}}{dt} = \frac{T_{\text{air}} - T_{\text{w,in}}}{R_{\text{w,air}}} + \frac{T_{\text{w,out}} - T_{\text{w,in}}}{R_{\text{w}}} + (1 - f_{\text{conv}}) \dot{Q}_{\text{h,SH}} \quad (25)$$

$$C_{\text{w}} \frac{dT_{\text{w,out}}}{dt} = \frac{T_{\text{w,in}} - T_{\text{w,out}}}{R_{\text{w}}} + \frac{T_{\text{amb,eq}} - T_{\text{w,out}}}{R_{\text{w,amb}}} \quad (26)$$

The set of ordinary differential equations describing the thermal dynamics of the building (Equations (24)-(26)) is discretized with a zero-order hold discretization and reformulated into a state-space system as:

$$\mathbf{x}[k+1] = \mathbf{A}\mathbf{x}[k] + \mathbf{B}\mathbf{u}[k] \quad (27)$$

$$y[k] = \mathbf{C}\mathbf{x}[k] \quad (28)$$

where the states vector contains the building's temperatures $\mathbf{x} = [T_{\text{air}} \quad T_{\text{w,in}} \quad T_{\text{w,out}}]^T$, the input vector comprises the controllable space heating input and the weather condition $\mathbf{u} = [\dot{Q}_{\text{h,SH}} \quad T_{\text{amb}} \quad \dot{q}_s]^T$, and the output is the indoor air temperature $y = T_{\text{air}}$. To exploit the TBM flexibility of the building, the comfortable indoor air temperature is interpreted as the allowed temperature range at each time step k described by the following Equation:

$$T_{\text{air,min}}[k] \leq T_{\text{air}}[k] \leq T_{\text{air,max}}[k] \quad (29)$$

By maintaining the indoor air temperature within a permitted range rather than a fixed temperature set point, the controllers can utilize the thermal storage of the TBM to increase energy flexibility.

2.1.7. Power balance

The power balance is defined as the equality between the generated and demanded power at each time step k (see Equation (30)). In addition to the previously defined variables, we introduce the purchased and sold power from/to the grid, defined as $P_{\text{buy}}[k]$ and $P_{\text{sell}}[k]$, respectively. The $P_{\text{el,load}}[k]$ represents the load of the building's electrical appliances generated as a typical curve for a family household. It is introduced to analyze the EMSs operation under comprehensive building load, consisting of flexible $P_{\text{el,HP}}$ and non-flexible $P_{\text{el,load}}$ parts:

$$P_{\text{PV}}[k] + P_{\text{buy}}[k] + P_{\text{el,FC}}[k] + P_{\text{d}}[k] = P_{\text{sell}}[k] + P_{\text{el,load}}[k] + P_{\text{el,HP}}[k] + P_{\text{ch}}[k] \quad (30)$$

2.2. Control algorithms

In this section, the developed control algorithms are described. Section 2.2.1 describes the optimal control of the building with DER based on MPC. Thereafter, the ComEMS4Build in Section 2.2.2 and the RBC in Section 2.2.3 are developed using the minimal inputs required and based on the features of optimal MPC behavior.

2.2.1. Optimal benchmark - Model Predictive Control (MPC)

The MPC utilizes the component models to forecast the behavior of the building. Based on this forecast, an optimization problem is solved to determine the control trajectory that minimizes the overall cost of the HESS. The cost comprises three parts: (i) the cost associated with the power exchange with the grid, (ii) the investment and lifecycle costs of the BESS and FC, and (iii) the on/off costs of the FC. In this case, the on/off costs represent the toggling of the FC, which also affects its lifespan. The MPC's objective function is defined as:

$$\begin{aligned} \min \sum_{k=1}^H t_s \cdot & \underbrace{(p_{\text{buy}}[k] \cdot P_{\text{buy}}[k] - p_{\text{sell}} \cdot P_{\text{sell}}[k])}_{\text{Costs of power exchange with grid}} + \underbrace{t_s \cdot (\sigma_{\text{B,ch}} \cdot P_{\text{ch}}[k] + \sigma_{\text{B,d}} \cdot P_{\text{d}}[k] + \sigma_{\text{FC}} \cdot s_{\text{FC}}[k])}_{\text{Lifecycle cost}} \\ & + \underbrace{\sigma_{\text{FC,on}} \cdot s_{\text{FC,on}}[k] + \sigma_{\text{FC,off}} \cdot s_{\text{FC,off}}[k]}_{\text{On/off cost}} \end{aligned} \quad (31)$$

subject to Equations (1)-(30)

where p_{buy} and p_{sell} represent the electricity tariff and remuneration price in €/kWh, respectively. The number of time steps in the MPC's prediction horizon is denoted as H . The $\sigma_{\text{B,ch}}$, $\sigma_{\text{B,d}}$ in €/Wh and σ_{FC} in €/h are the utilization costs consisting of the investment σ_{in} in € and operation and maintenance costs σ_{om} €/h (see Equation (32)). The lifespan of the BESS and FC in h are presented with L_{B} and L_{FC} , respectively. As the lifespan of the battery is not given by the datasheet, it is estimated based on Depth of Discharge cycles (DoD) and the battery's capacity E_{max} , Equation (33), as described in [3]. On the other hand, the FC lifecycle can be found in the datasheet:

$$\sigma_i = \sum_i \frac{1}{\eta_i} \left(\frac{\sigma_{\text{in},i}}{L_i} + \sigma_{\text{om},i} \right), \quad i \in \{\text{"B,ch"}, \text{"B,d"}, \text{"FC"}\} \quad (32)$$

$$L_{\text{B}} = \frac{E_{\text{max}}}{P_i} \cdot N_{\text{B}} \quad i \in \{\text{"ch"}, \text{"d"}\} \quad (33)$$

The $\sigma_{\text{FC,on}}$ and $\sigma_{\text{FC,off}}$ are costs of toggling the FC in €. With respect to this, $s_{\text{FC,on}}$ and $s_{\text{FC,off}}$ indicate whether the FC is starting or stopping, defined by the logic of Equation (34):

$$\begin{aligned} s_{\text{FC,on}}[k] &= s_{\text{FC}}[k] \wedge (\neg s_{\text{FC}}[k-1]) \\ s_{\text{FC,off}}[k] &= s_{\text{FC}}[k-1] \wedge (\neg s_{\text{FC}}[k]) \end{aligned} \quad (34)$$

The MPC employs the models described in Section 2.1 as control models, except for the nonlinear model of the H_2 system. The nonlinearity in Equations (7) and (8) arises because the electrical efficiency $\eta_{\text{el,FC}}$ is a function of the FC power consumption. This nonlinearity causes convergence issues for the optimization, which is avoided by approximating the electrical efficiency $\eta_{\text{el,FC}}$ with a constant value estimated from the datasheet, as already reported

in the literature [12]. Since the MPC's horizon time is 24 h, MPC gets its permissible amount of H_2 that it can utilize throughout the day, by dynamically defining the LOH_{\min} for each day:

$$\Delta LOH = \frac{24h \cdot LOH_{\text{init}}}{N} \quad (35)$$

if $N \bmod k = 0$ then

$$LOH_{\min} = LOH_{\max} - \Delta LOH \cdot \text{Number of the day} \quad (36)$$

where N defines the number of steps for the whole winter, e.g., the entire simulation period. The LOH_{init} denotes the initial state of the H_2 storage, while 'Number of the Day' refers to the order of the day in the simulation. In this way, the MPC must hold on to a minimum constraint, but it doesn't need to empty the H_2 storage to daily LOH_{\min} unless necessary.

2.2.2. Comfort-Oriented Energy Management System for Residential Buildings (ComEMS4Build)

In contrast to the MPC, the FLC, as a soft-computing algorithm, does not require models for operation. The advantages of the FLC increase as energy systems become more complex, since it does not depend on modelling forecasts. The FLC features the ability to manage uncertainties, imprecision, and noisy inputs effectively [14]. The building parameters, such as indoor air temperature T_{air} , or external parameters, e.g., electricity price signal p_{buy} can be presented as soft linguistic variables in FLC, describing the current or future state of the system. The fuzziness allows for partial truth, with the conclusions, i.e., control outputs, being derived based on the activated *if-then* rules. The idea behind the ComEMS4Build is to hierarchically split the flexible load management and operation of HESS, as shown in Figure 2 (left). From the HESS side, first, the FC is controlled to determine, based on previous states, whether it is reasonable to turn it on. Hereafter, the BESS is controlled, which should support the FC either by charging or discharging. The ComEMS4Build consists of two main parts: defining the flexible heating load and managing the HESS. The flexible heating load is operated with FLC_{flex} , which is based on the following inputs: (i) HESS states SOC and LOH, (ii) current solar radiation \dot{q}_s , (iii) indoor air temperature state χ_{SH} , (iv) DHW storage state χ_{DHW} , and (v) empirical distribution function (EDF) of the next 24-hours electricity prices, \hat{p}_{buy} . Based on these inputs, FLC_{flex} determines the intensity of the flexible heating load.

The thermal states of SH χ_{SH} and DHW χ_{DHW} are defined as follows:

$$\chi_{\text{sh}} = \sqrt{\frac{T_{\text{air}}[k-1] - \max(T_{\text{air,min}}[k], T_{\text{air,min}}[k+5])}{T_{\text{air,max}}[k] - \max(T_{\text{air,min}}[k], T_{\text{air,min}}[k+5])}} \quad (37)$$

$$\chi_{\text{DHW}} = \left(\frac{V_{\text{DHW}}[k-1] - V_{\text{DHW,min}}}{V_{\text{DHW,max}} - V_{\text{DHW,min}}} \right)^2 \quad (38)$$

where the $T_{\text{air,min}}[k+5]$ represents the minimal temperature bound in the next five hours, defined by Equation (40), used to preheat if necessary. The state of the indoor air temperature χ_{sh} is under the square root to control the temperature, relatively near to the $T_{\text{air,min}}$. In contrast, the DHW state χ_{DHW} is squared to control the volume of the DHW storage to be closer to $V_{\text{DHW,max}}$ as the future demand is not known and to secure the storage if a greater DHW demand appears. The empirical distribution function of electricity prices is defined by Equation (39):

$$\hat{p}_{\text{buy}}[k] = \hat{F}_n(p_{\text{buy}}[k]) = \frac{1}{H} \sum_{i=k+1}^{k+H} I(X_i \leq p_{\text{buy}}[k]) \quad (39)$$

where $\hat{F}_n(x)$ is the proportion of the dynamic electricity prices that are less than or equal to $p_{\text{buy}}[k]$, in step k , on a horizon of $H = 24$ h. The X_i represents the observed electricity prices, while $I(\cdot)$ indicates whether the condition is true. The defined flexible load $P_{\text{el,HP}}$ by FLC_{flex} is first summed with the non-flexible electrical load $P_{\text{el,load}}$, which comes from electrical appliances in the household. Then PV generation is used to cover part or the entire load if possible. The residual is calculated as $\Delta P[k] = P_{\text{PV}}[k] - P_{\text{el,HP}}[k] - P_{\text{el,load}}[k]$. If there is residual load the FLC_{FC} defines the amount that can be covered by FC based on:

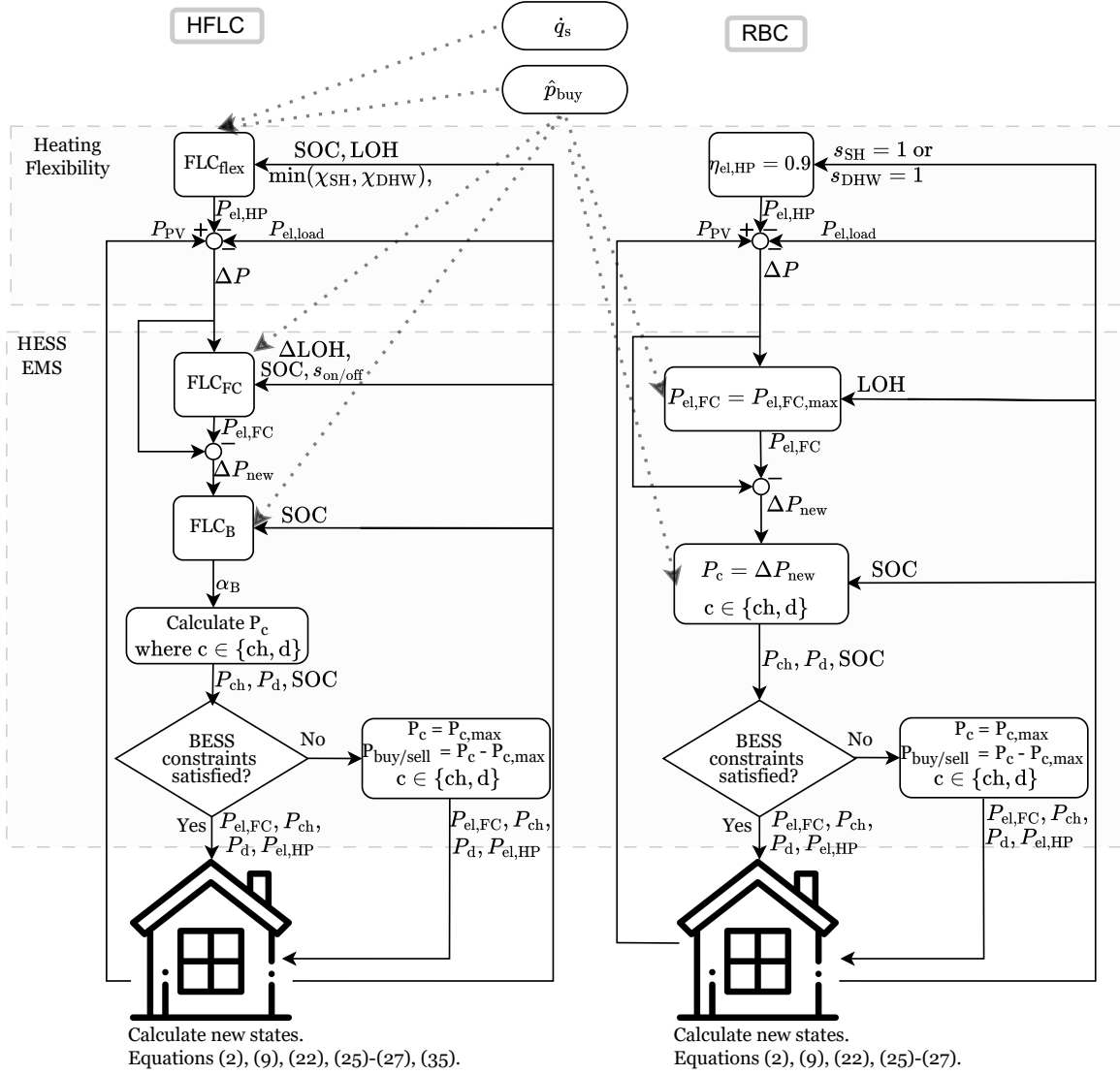


Figure 2: The flowcharts for ComEMS4Build (left) and RBC (right) showing the information flow and data required for operation.

- EDF price signal \hat{p}_{buy} , where the FC is switched on when the prices are highest throughout the day
- toggling state $s_{\text{on/off}}[k-1]$ of the FC in the last time step
- state of the HESS as SOC and a permissible amount of H_2 usage throughout the day ΔLOH .

The daily permissible amount of H_2 ΔLOH is for ComEMS4Build defined by (35). This value is updated daily, as ComEMS4Build may not use the entire permissible amount unless necessary. The FLC_{FC} controller is only used in case the load $\Delta P[k]$ is negative. If $\Delta P[k]$ is positive, the FC is not in operation. The output of the FLC_{FC} is the amount of power that FC can produce for current demand. The BESS is controlled with FLC_{B} and with the lowest inputs required:

- residual of the required power to satisfy the demand fully $\Delta P_{\text{new}}[k] = \Delta P[k] - P_{\text{el,FC}}[k]$
- EDF electricity price signal \hat{p}_{buy}

- state of the charge of BESS SOC.

If the BESS cannot meet the demand, either due to charging or discharging power constraints or due to an empty/full storage, the corresponding residual is bought from or sold to the grid. The output of FLC_B is defined as factor $\alpha_B \in [-1, 1]$. Its sign indicates whether the BESS is being charged (positive) or discharged (negative). For example, if the load ΔP_{new} is negative, indicating there is still residual demand to cover, and $\alpha_B \geq 0$, the entire residual demand will be purchased from the grid. If needed, the BESS will be charged additionally, as electricity prices are currently favorable. For this, the factor's value $\alpha_B \in [0, 1]$ decides the amount that will be purchased for the BESS charging. However, $\alpha_B \leq 0$ indicates the BESS discharging. The factor α_B determines the amount discharged from the BESS $P_d = \alpha_B \cdot \Delta P_{\text{new}}$ and the amount purchased $P_{\text{buy}} = (1 - \alpha_B) \cdot \Delta P_{\text{new}}$. Additional description of the structure of FLC_{flex} , FLC_{FC} and FLC_B is discussed in Appendix A.

2.2.3. Rule Based Controller (RBC)

The RBC is based on the ComEMS4Build workflow and is designed to require minimal inputs, as shown in Figure 2 (right). Namely, first the thermal states χ_{SH} and χ_{DHW} are defined. In this context, the same Equations (37) and (38) are used as for the ComEMS4Build, except that RBC does not have inputs about the future bound temperature $T_{\text{air,min}}[k+5]$, and both thermal states are compared equally. After defining the flexible load and whether the PV generation P_{PV} can cover the load, it is considered whether the FC should be switched on. This decision is based on whether the demand exists, i.e., $\Delta P < 0$, and whether the EDF electricity prices are in the upper quartile, e.g., the electricity prices are the highest in the current step. If so, the FC is turned on with maximal permissible power $P_{\text{el,FC}} = P_{\text{el,FC,max}} \cdot \zeta$. Therefore, the residual power is calculated, which is used for charging or discharging the BESS. However, if the EDF electricity prices are in the lowest quartile, i.e., current electricity prices are favorable, the BESS is charged if needed and the load, if it exists, is purchased from the grid.

2.2.4. Inputs required for each EMS

Table 1 gives an overview of the inputs required by each scheduler. The forecasting models include those for each component, such as PV, HESS, DHW storage, HP, and building model. Moreover, forecasting profiles are weather, DHW thermal load, and appliances' electrical load. The MPC requires both forecasting models and profiles. Future temperature bounds, $T_{\text{air,min}}$ and $T_{\text{air,max}}$, are user-defined temperature ranges required by MPC for 24 hours ahead. ComEMS4Build requires only 5 hours ahead of indoor air temperature bounds, which is just enough to preheat if necessary. Day-ahead electricity prices, which are required for each schedule, are not considered as a prediction. Instead, they are established in advance for the following day [43]. The current weather T_{amb} and \dot{q}_s is required by MPC, while ComEMS4Build uses only the current solar radiation \dot{q}_s for taking the actions about flexible heating. As expected, all three controllers require the current indoor air temperature T_{air} , volume of usable hot water in DHW storage V_{DHW} , and state of the HESS, i.e., SOC and LOH. The previous state of the FC and permitted daily H_2 usage, i.e., ΔLOH , is required by ComEMS4Build and MPC.

Table 1: The inputs required by the schedulers.

Required inputs	Forecasting models	Forecasting profiles	Future temp. bounds	24-ahead el. tariffs	T_{amb}	\dot{q}_s
RBC				✓		
ComEMS4Build			✓	✓		✓
MPC	✓	✓	✓	✓	✓	✓
Required inputs	T_{air}	V_{DHW}	SOC	LOH	ΔLOH	$s_{\text{on/off}}$
RBC	✓	✓	✓	✓		
ComEMS4Build	✓	✓	✓	✓	✓	✓
MPC	✓	✓	✓	✓	✓	✓

3. Evaluation Setup

This section describes the data and profiles utilized in the present study. The scenarios are evaluated for twelve winter weeks in Germany, with weather and electricity price data from December 2022 to February 2023. All models are implemented in Python, where the MPC utilizes the Gurobi optimizer [44]. The simulation resolution is 1 h for all controllers, while the MPC prediction horizon is 24 h. It is assumed that by using the EL, the system is capable of replenishing the H_2 storage during periods of high solar radiation, i.e., during the summer in Germany. Then, in winter, the schedulers can discharge the H_2 storage. Thus, at the beginning of the simulation, the H_2 storage is assumed to be filled up to the maximum $E_{H_2, \max}$ with green H_2 produced during the summer months, while the BESS SOC is set to 50%.

3.1. Input data

The demand profiles utilized in the present paper are DHW demand $\dot{Q}_{\text{dm,DHW}}$ and electricity demand $P_{\text{el,load}}$. The DHW demand $\dot{Q}_{\text{dm,DHW}}$ is generated using the DHWCalc tool [45], designed to generate DHW profiles, utilizing statistical methodologies. The electricity load $P_{\text{el,load}}$ of the appliances in the building is generated using the LPG tool [46] by setting the parameters for a typical four-person household, consisting of two parents with two children. The hourly dynamic electricity tariffs p_{buy} for Germany are obtained from aWATTar [43]. The electricity prices are composed of a constant base price and a variable price signal predefined for the day-ahead market. In contrast, the remuneration price is constant $p_{\text{sell}} = 7.94$ cent/kWh and is retrieved from the German Federal Grid Agency (*Bundesnetzagentur*) [47]. The meteorological data are retrieved from the German Weather Service [48] at a 10-minute resolution. In particular, the following factors are taken into consideration: the ambient air temperature T_{amb} , global solar radiation \dot{q}_s , and diffuse solar radiation. The meteorological data is retrieved from the weather station in Rheinstetten, Germany, which was selected as the nearest location to the city of Karlsruhe with available data. The input data snapshot is depicted in Figure 3.

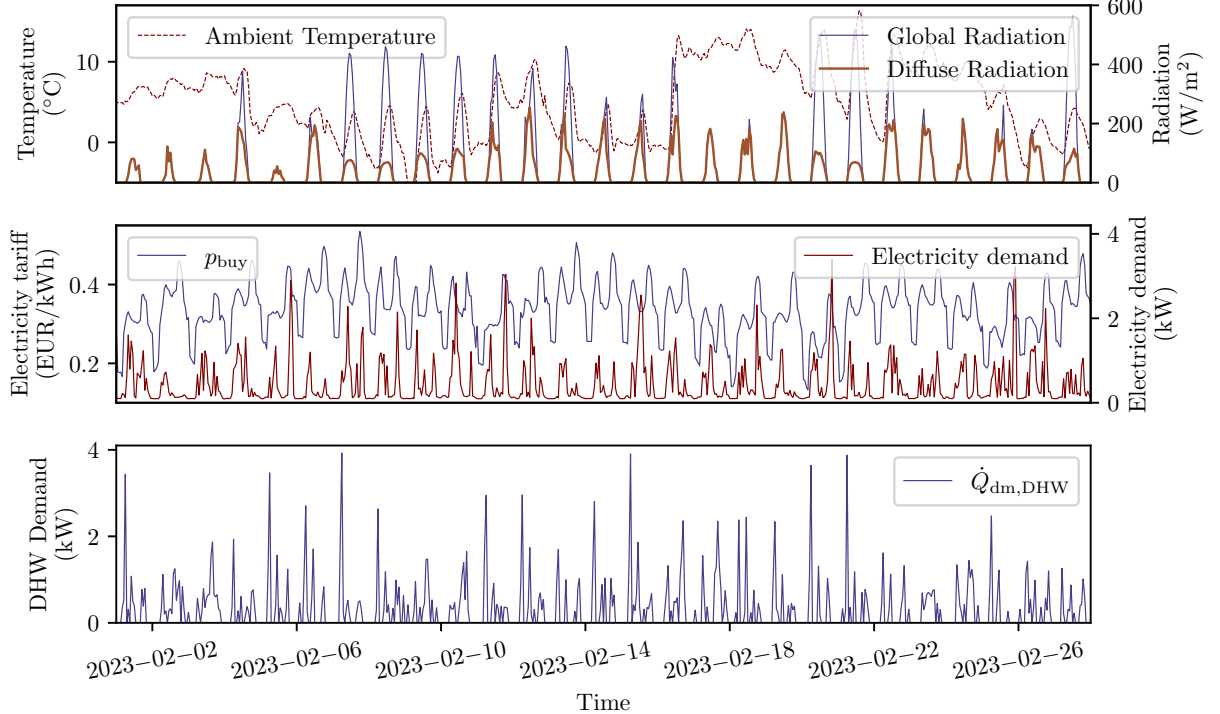


Figure 3: Input data snapshot for February 2023.

The occupancy schedule is further derived from [49], where the schedule differs according to the day of the week - *weekday* and *weekend* and occupancy type, categorized as follows: *at home*, *sleeping* and *away*. The lower bound temperature $T_{\text{air,min}}$ is detailed in Equation (40), while the upper bound $T_{\text{air,max}}$ is kept at 24 °C for all cases:

$$T_{\text{air,min}}[k] = \begin{cases} 21^{\circ}\text{C} & \text{if } \textit{home} \\ 18^{\circ}\text{C} & \text{if } \textit{sleeping, away} \end{cases}$$

$$\text{for } \textit{home} = \begin{cases} [6 \text{ AM}, 8 \text{ AM}) \cup [5 \text{ PM}, 11 \text{ PM}) & \text{if } \textit{weekday} \\ [6 \text{ AM}, 11 \text{ PM}) & \text{if } \textit{weekend} \end{cases} \quad (40)$$

$$\textit{sleeping, away} = \begin{cases} [23 \text{ PM}, 6 \text{ AM}) \cup [8 \text{ AM}, 5 \text{ PM}) & \text{if } \textit{weekday} \\ [23 \text{ PM}, 6 \text{ AM}) & \text{if } \textit{weekend} \end{cases}$$

$$T_{\text{air,max}}[k] = 24^{\circ}\text{C} \quad (41)$$

3.2. Thermal building parameters

The thermal building parameters are identified based on one building of the Living Lab Energy Campus located on Campus North of the Karlsruhe Institute of Technology [50]. The parameter set is for highly insulated buildings, where the parameter identification and validation are evaluated during the German winter months and are described in detail in [42].

3.3. DHW storage parameters

The DHW demand for a 4-person household is 200 l/day based on [51]. Accordingly, the storage size is selected as $V_{\text{DHW,max}} = 300 \text{ l}$ to cover this demand. Standing losses are $Q_{\text{L,DHW}} = 35 \text{ W}$ as the storage is chosen to be the A+ efficiency level according to EU regulation 814/2013 [52]. The temperature of the DHW storage T_{DHW} is set to 45 °C, as shown in Table 2. The DHW storage system is not employed for direct utilization; rather, it functions as a heat storage. Through the utilization of a heat exchanger, the stored heat is transferred to the fresh water supply. Thus, the temperature of the DHW storage system can be reduced, thereby circumventing any potential hygiene-related issues [41]. Moreover, the heat recovery from the FC is also appropriate in this case, given that the water in the storage is technical water and not drinking water [53].

3.4. HP parameters

The HP chosen for this use case is the air-source LG Therma V Monobloc type HM051M U43 [54] with a heating capacity of 5 kW. As already mentioned, the DHW is kept at 45 °C. In addition, SH is heated to 55 °C using an underfloor heating system. The COP varies from 1.93 to 5.16 for 45 °C and from 1.6 to 4.15 for 55 °C for outside temperatures T_{amb} between -15 °C and 20 °C.

3.5. Renewable energy system

The PV and BESS parameters are based on the equipment of the experimental building from which the temperature measurements are retrieved and are provided in Table 2. The electrical part of the FC parameters is based on the datasheet Horizon Educational FC H-2000 [55]. Since FC power over 80% of its maximum power highly impacts the degradation of the system, its power is additionally restricted with a security factor $\zeta = 80\%$ of its maximum [33, 56]. Full autarky would lead to a notable increase in HESS, since the peaks in the worst-case scenarios would need to be covered. From the investment side, it is more effective to utilize the grid during such demand peaks. Therefore, we chose a dimension of the H_2 storage that could cover half of the daily electricity demand (HP heating and appliances), over the winter months. Based on the average FC efficiency, the required amount of H_2 is calculated and presented in Table 2. The overall efficiency of the FC system with heat recovery is assumed to be $\eta_{\text{FC}} = 75\%$ based on the study by Gandiglio et al. [22]. Furthermore, we evaluate the heat recovery (see Section 4.5) if the overall FCs system efficiency could achieve the $\eta_{\text{FC}} = 90\%$ as discussed in [9, 10]. It should also be noted that EL is not considered in the present study because it would not be optimal to operate it during the German winter when demand is at its peak and solar radiation is low.

Table 2: PV, BESS, DHW storage and H_2 system parameters.

Component	Variable	Value	Variable	Value
PV	n_{module}	30	η_{STC}	0.19
	a_{module}	1.685 m ²	$NOTC$	50 °C
	η_T	0.005 °C ⁻¹	T_{STC}	25 °C
	$\eta_{L\&T}$	0.9		
BESS	E_{max}	6.5 kWh	$P_{d,\text{max}}$	1 kW
	η_{ch}	0.93	SOC_{min}	0.1
	η_d	0.93	SOC_{max}	0.9
	$P_{\text{ch,max}}$	1 kW	SOC_{init}	0.5
DHW Storage	$V_{\text{DHW,max}}$	300 l	$V_{\text{DHW,min}}$	40 l
	\dot{Q}_l	35 W	T_{DHW}	45 °C
H_2 system	$P_{\text{FC,max}}$	2441.6 W	$P_{\text{FC,nom}}$	2000 W
	$P_{\text{FC,min}}$	399.2 W	$\eta_{\text{FC,sys}}$	0.75
	$E_{H_2,\text{max}}$	1800 kWh	LOH_{init}	1

According to [57], major degradation mechanisms of H_2 components relevant for supervisory EMS include on–off cycling and power fluctuations, where steady-state operation of the FC can extend its lifespan by a factor of 12–18 compared to dynamic operation. Given the high initial investment costs, the undesirable behavior of the FC is important to be taken into consideration in EMS. Table 3 presents the degradation costs for the HESS system, where $\sigma_{\text{in,FC}}$ and $\sigma_{\text{in,B}}$ represent the initial investment costs for the HESS measured in €. Lifespan of the FC is defined with L_{FC} , while operational and maintenance costs (OM) of the FC are defined as $\sigma_{\text{om,FC}}$. The lifetime of the BESS can not directly be found in datasheets, but rather needs to be calculated based on the DoD cycles N_B . The lifespan can then be calculated as described in [3]. The above-mentioned investment costs, FC lifespan, and BESS’s DoD N_B are solely based on the datasheets of corresponding components [58, 59]. The OM for the BESS is assumed to be negligible, while the OM of the FC is defined in [12]. Furthermore, the ON/OFF costs of the H_2 components are defined with $\sigma_{\text{FC,on}}$, $\sigma_{\text{FC,off}}$.

Table 3: Degradation costs of HESS based on [12, 58, 59].

Component	Variable	Value	Variable	Value
FC	$\sigma_{\text{in,FC}}$	10908 €	$\sigma_{\text{om,FC}}$	0.038 €/h
	L_{FC}	35000 h	$\sigma_{\text{FC,on}}$	0.10 €
	$\sigma_{\text{FC,off}}$	0.053 €		
BESS	$\sigma_{\text{in,B}}$	900 €	N_B	6000 cycles

3.6. Evaluation metrics

The comfort-oriented metrics utilized are thermal discomfort, electricity, and reimbursement costs. These metrics exhibit a trade-off relationship where improving one typically leads to a decline in the other. The objective is to minimize discomfort and operational costs simultaneously. The weekly average thermal discomfort d_{we} , Equation (42) is calculated by multiplying the intensity of the temperature bounds violation $T_{\text{air,min}}$ or $T_{\text{air,max}}$ by the duration of the violation [60]. The weekly energy costs $c_{\text{we,buy}}$ and reimbursement costs $c_{\text{we,sell}}$ are calculated as the sum of the purchased P_{buy} or sold P_{sell} electricity multiplied by the current electricity price p_{buy} or reimbursement price p_{sell} .

respectively:

$$d_{we} = t_s \cdot \sum_{k=1}^M d_k \quad (42)$$

$$d_k = \begin{cases} T_{air,min}[k] - T_{air}[k] & \text{if } T_{air,k} < T_{air,min}[k] \\ T_{air}[k] - T_{air,max}[k] & \text{if } T_{air}[k] > T_{air,max}[k] \\ 0 & \text{else} \end{cases}$$

$$c_{we,i} = t_s \cdot \sum_{k=1}^M p_i[k] \cdot P_i[k] \quad \text{for } i \in \{"buy", "sell"\} \quad (43)$$

where M represents the number of time steps in a week. The HESS and grid usage are evaluated weekly by multiplying the produced or consumed energy by sampling time t_s , Equation (44). The following are observed: weekly battery charged energy $P_{B,ch}$, battery discharged energy $P_{B,d}$, FC generation P_{FC} , purchased P_{buy} and sold energy P_{sell} and heat recovered $\dot{Q}_{FC,hr}$:

$$E_{we,i} = t_s \cdot \sum_{k=1}^M P_i[k], \quad \text{for } i \in \{"B,ch", "B,d", "FC", "buy", "sell"\} \quad (44)$$

$$E_{we,hr} = t_s \cdot \sum_{k=1}^M \dot{Q}_{FC,hr}[k] \quad (45)$$

Moreover, due to the high degradation of the FC, we evaluate the total working hours and the number of times the device is switched on and off for all three controllers. The working hours are obtained by multiplying the binary variable indicating that the FC is working s_{FC} by sampling time t_s over N number of time steps, Equation (46). The number of times the device is switched on and off is the sum of the binary variables indicating that the FC has changed the state from "off" to "on" $s_{FC,on}$ over N time steps, Equation 47:

$$WH_{FC} = t_s \cdot \sum_{k=1}^N s_{FC}[k] \quad (46)$$

$$T_{on/off} = \sum_{k=1}^N s_{FC,on}[k] \quad (47)$$

4. Experimental Results

This section describes the results obtained for the entire evaluation period, comparing the ComEMS4Build to the optimization-based scheduler, MPC, and the simple RBC. ComEMS4Build and RBC feature minimalistic inputs integrated in the algorithms, while MPC achieves optimality by integrating forecasting models.

4.1. Time series comparison

Figure 4 presents the exemplary three-day performance of all three controllers with high peaks of dynamic tariffs, and low solar radiation throughout the days. The upper plot row depicts the room air temperature T_{air} and volume of the DHW storage V_{DHW} . The dashed gray lines represent the minimal and maximal air temperature, $T_{air,min}$ and $T_{air,max}$, respectively, defined by Equation (40). The second row of subplots illustrate the electricity generation and consumption, particularly PV generation and total electricity demand consisting of electrical appliances $P_{el,load}$ and the HP's power demand $P_{el,HP}$. The third row represents the exchange with the grid, i.e., power sold to the grid, and purchased power from the grid. The right axis of this plot illustrates the electricity tariffs of the primary grid, thereby facilitating an understanding of the actions employed by the controllers. The latter two rows demonstrate the HESS utilization with the SOC and LOH of the HESS, as well as the power consumed or provided to the corresponding system.

When comparing the indoor air temperature T_{air} , it can be concluded that MPC keeps the indoor air temperature mostly at the lower bound, $T_{\text{air,min}}$. At the same time, RBC, as constructed, heats the room to the upper bound $T_{\text{air,max}}$ and then cools down to the lower bound, $T_{\text{air,min}}$, thereby evoking indoor air temperature fluctuations, whereas the ComEMS4Build algorithm maintains a balanced temperature. When it comes to the volume of the DHW storage V_{DHW} , the ComEMS4Build and RBC are keeping the volume more likely over 50% of the storage, since they both do not know the DHW demand. In contrast, MPC, having the perfect DHW demand forecast, maintains the volume just enough to meet near-future demand. However, this situation would not be realistic as the DHW demand is inherently stochastic. Examining the electricity plot, all three controllers utilize the HESS when electricity prices are high, thereby attempting to relieve the main grid. However, in periods of lower demand, such as between 9 AM on December 3rd and 1 AM on 4th, when high electricity prices prevail, the RBC activates the FC to its maximum capacity. Since demand is lower, the BESS is charged using the residual power, and any remaining power is sold. This occurrence can be attributed to the fact that the RBC possesses only limited inputs regarding the demands. In the event of a minor demand arising and high electricity prices, the system initiates the FC, as the BESS has been discharged. This is executed in order to satisfy the demand by utilizing the HESS, particularly in instances where the primary grid is experiencing overload. However, the MPC sells less energy, as it finds it more optimal to utilize it within the building. When electricity prices are low, for example, during the night between December 4th and 5th, all three controllers use the main grid to meet demand, charge the BESS, or satisfy demand as needed. Notably, MPC utilizes the main grid the most when prices are lower, with high purchased power peaks, e.g., on 4th December, reaching up to 5.1 kW. In contrast, such occurrences are less frequent for ComEMS4Build and RBC.

Another example of the comparison is when there is high PV generation and the electricity prices are reaching low values, e.g., 0.23 €/kWh, see Figure 5. It can be seen that both the MPC and ComEMS4Build utilize the TBM as thermal storage during periods of excess PV generation. However, the ComEMS4Build slightly violates the upper temperature bound $T_{\text{air,max}}$, as it lacks a hard constraint like the MPC. The temperature bounds for ComEMS4Build are instead used as inputs for locating the indoor air temperature in the range $[T_{\text{air,min}}, T_{\text{air,max}}]$ (see Equation (37)). Conversely, RBC has no input regarding PV generation, thus it exerts minimal influence on the indoor air temperature. As the Figure 5 shows, after two months of the evaluation period, the H_2 storage is filled with less than 30% of H_2 for MPC and ComEMS4Build, while the RBC has depleted the H_2 storage to the LOH_{min} 16 days before the end of the evaluation. Meaning, RBC did not have a H_2 for 19% of the evaluation period. This happened due to the lack of additional input and limitations on H_2 usage. Moreover, under these favorable conditions, the MPC primarily utilizes the HESS rather than the primary grid. In addition to storing energy in the TBM, it utilizes PV generation to charge the BESS. In these conditions, it can be observed that the BESS is charged to full capacity and then discharged until it is depleted throughout the day. For the ComEMS4Build, that is not the case; it uses the main grid when the prices are lowest. The RBC utilizes these favorable conditions the least, primarily relying on the main grid and also selling the excess energy generated by PV.

4.2. Occupant-oriented metrics

From the occupant side, the discomfort defined in Equation (42) and electricity costs and reimbursement in Equation (43) are evaluated weekly and presented in Figure 6. MPC fulfills the occupants' comfort without any comfort violation. Similarly, ComEMS4Build exhibits no thermal discomfort in 10 out of 12 weeks. In the rest two weeks it experiences discomfort of 0.68 Kh and 2.14 Kh due to the excess solar energy in the days when it can not further capture this energy in the TBM or in a BESS (see Figure 5). In these cases, it increases the indoor air temperature up to $T_{\text{air,max}}$ with slight violation of constraints. The RBC has the biggest discomfort median of 0.68 Kh, but still reasonable. It switches off the heating when it reaches $T_{\text{air,max}} = 24^\circ\text{C}$ and turns on when it cools down to $T_{\text{air,max}} = 21^\circ\text{C}$. In these moments, when temperatures reach these levels, it always slightly deviates above or below the respective value. Moreover, RBC consistently prioritizes heating DHW storage over SH.

MPC achieves median weekly electricity costs of 12.96 €. The ComEMS4Build and RBC have similar ranges of electricity costs. However, ComEMS4Build has a lower median value of 25.02 € compared to RBC with 43.10 €. In two weeks, MPC reaches high electricity costs of 64.35 € and 61.24 €. These weeks are featured with high electricity prices and low PV generation (see Figure 4). In these cases, ComEMS4Build also reaches the highest costs of 88.21 € and 79.24 €. For RBC, these costs are among the three highest weekly costs, at 91.67 € and 77.90 €, respectively. None of the three schedulers obtains a notable reimbursement from selling the energy. MPC has the median of 0 €, ComEMS4Build of 0.66 € and RBC of 2.84 € for reimbursement costs weekly. As can be observed, the MPC attempts

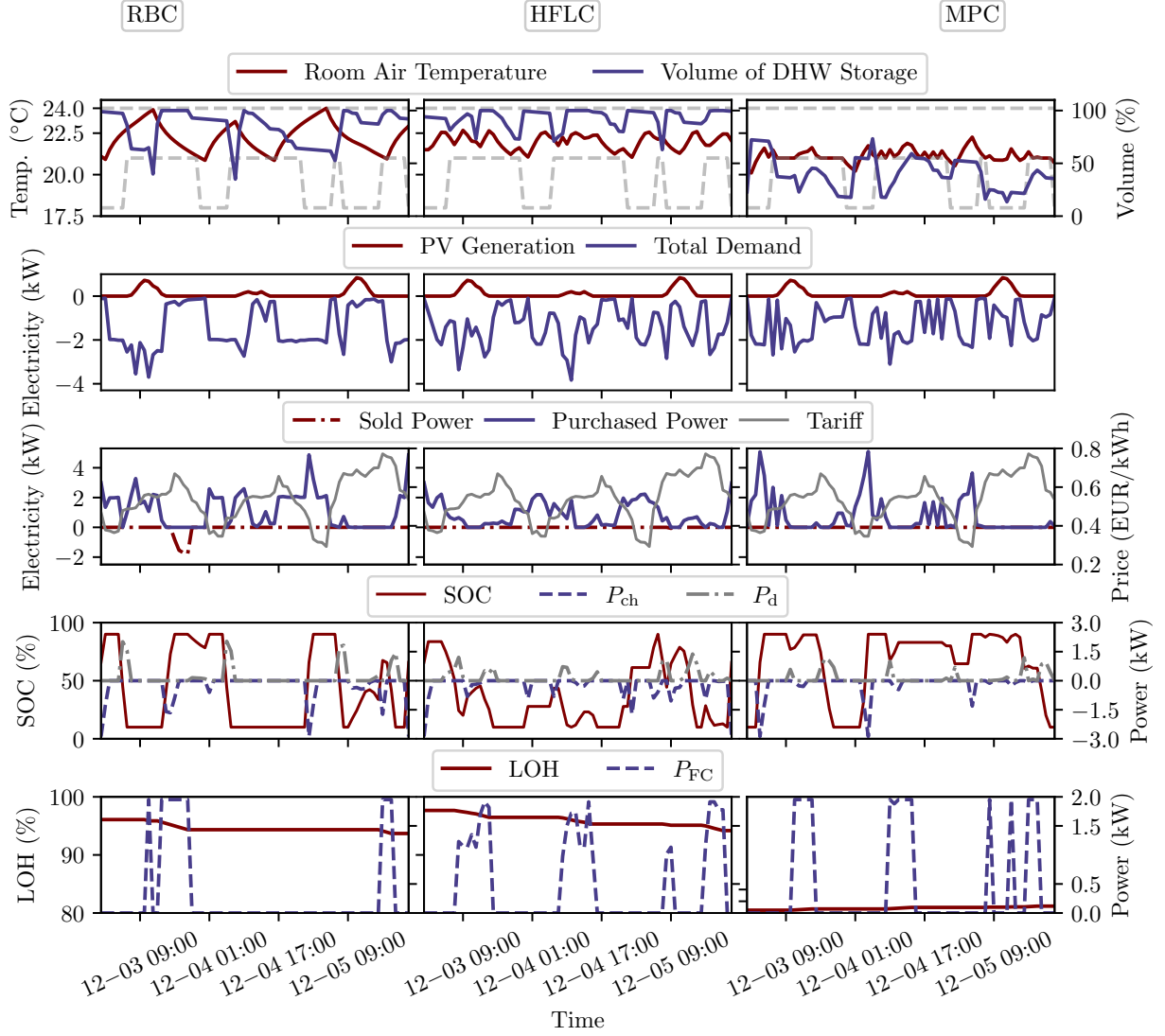


Figure 4: Example of a three-day performance comparison of all three controllers, taken from the twelve-week simulation carried out.

to utilize the entire PV-generated energy for either thermal or electrical storage, as it does not find it optimal to sell it at the reimbursement price of $p_{\text{sell}} = 7.94$ cent/kWh.

Since the HP is utilized for both SH and DHW, each scheduler needs to manage both types of thermal demands. As the SH demand is a flexible demand, the DHW demand is generated as a non-flexible profile demand. However, the DHW storage provides flexibility from the DHW perspective. Both ComEMS4Build and RBC give priority to the DHW over an SH, as they lack input about future DHW demand. Thus, they both keep the storage filled mostly at more than 50%. In contrast, MPC manages demand through ideal forecasting, ensuring the storage is filled enough to cover near-future demand. This makes ComEMS4Build and RBC schedulers more robust to DHW demand changes, while MPC can be fragile to changes when the forecast is not ideal. In the current setup, all three schedulers fulfill the demand in each time step.

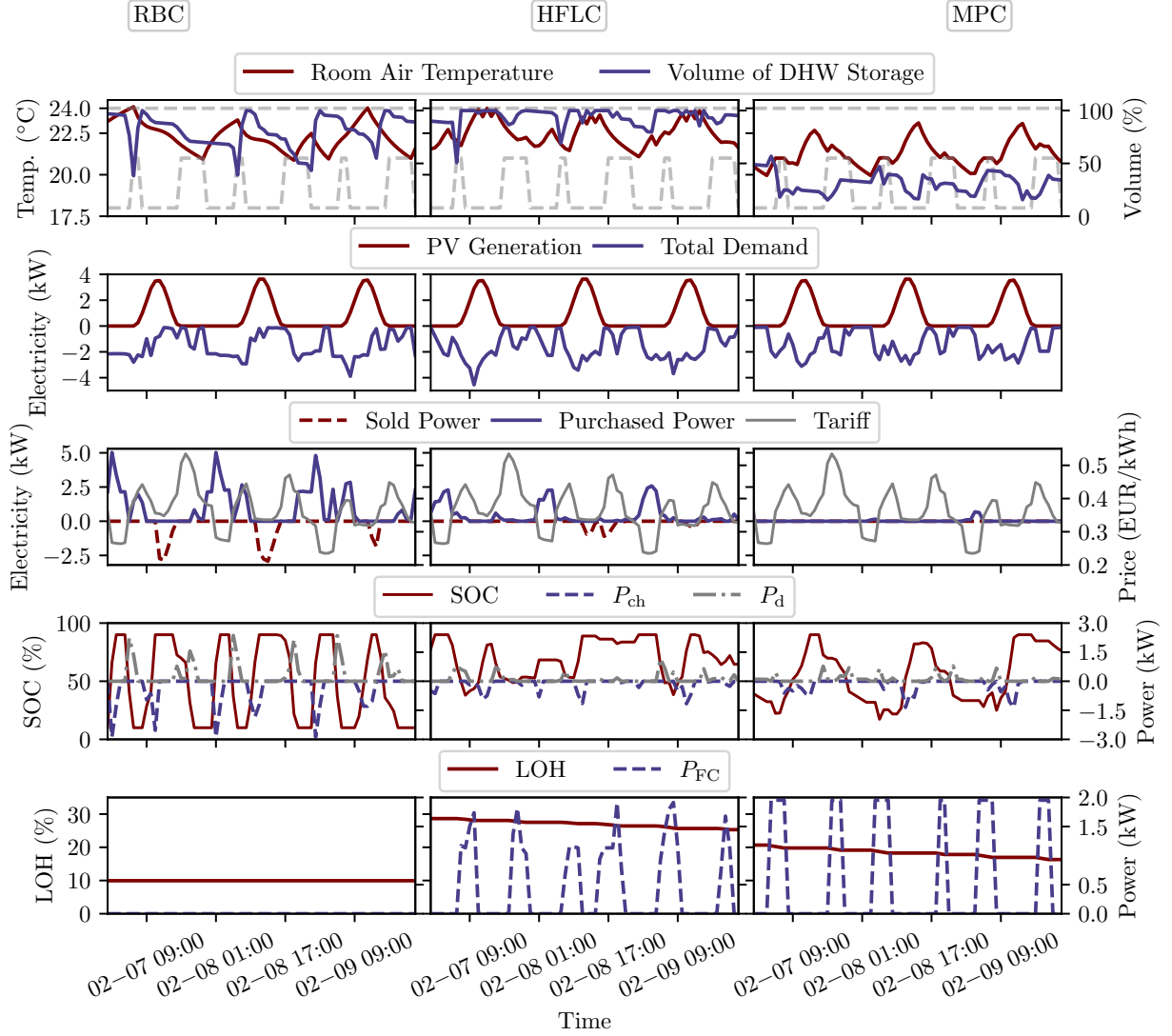


Figure 5: Example of a three-day performance comparison of all three controllers with high PV generation and troughs of up to 0.23 €/kWh in electricity tariffs.

4.3. HESS utilization

Figure 7 compares the HESS utilization of RBC and ComEMS4Build with optimization-based MPC on a weekly basis in a box plot depicting the BESS charging, and H_2 consumption, respectively. When it comes to the weekly charged energy, the ComEMS4Build exhibits behavior more similar to the MPC than the RBC. However, the MPC uses the least BESS with a median of 27.15 kWh per week, while the RBC uses the most with a median of 49.57 kWh per week. The ComEMS4Build exhibits behavior similar to the MPC, with a median of 27.44 kWh for weekly charging. The RBC operates the FC on its maximum permissible power $P_{el,FC} = \zeta \cdot P_{el,FC,max}$ and thus relies on the BESS when the FC is activated; after meeting the instantaneous demand, any surplus power is directed to charging the BESS. In contrast, the ComEMS4Build does not control the FC on maximum power, enabling more informed power management decisions. The third plot depicts the H_2 consumption, with the ComEMS4Build showing the least difference in consumption between weeks, ranging between 54.11 kWh and 78.54 kWh, and the MPC showing the most, ranging between 23.44 kWh up to 123.08 kWh. Meaning, the ComEMS4Build exhibits the most robust H_2

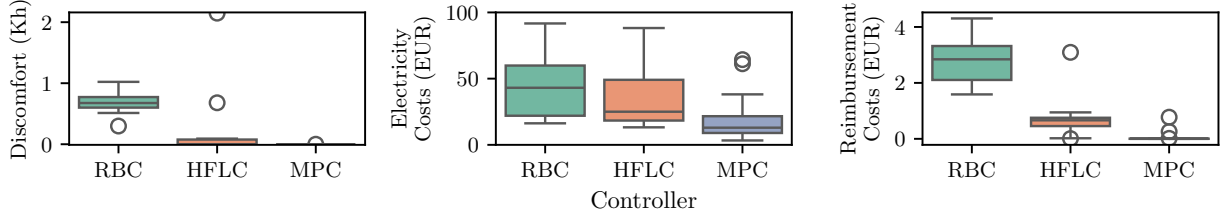


Figure 6: Comfort violation, electricity, and reimbursement costs depicted for the whole winter period and evaluated weekly.

consumption, characterized by low dependence on external factors, whereas the MPC has the opposite. The electricity price signal mainly impacts the variation in H_2 usage by MPC. It uses less H_2 when prices are extremely low, i.e., less than 0.2 €/kWh. Conversely, given the days with much higher prices, it utilizes the FC more often.

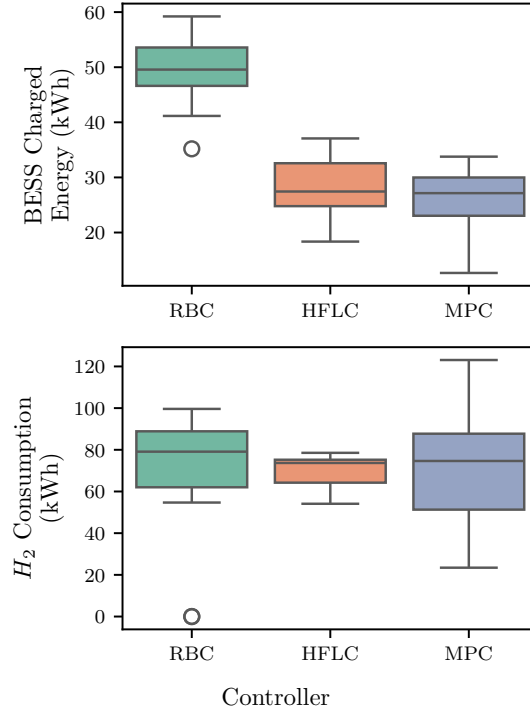


Figure 7: Renewables weekly usage for all three controllers. Weekly BESS charged energy is presented on the top subplot, while H_2 consumption is presented as consumed energy on the bottom subplot.

The FC degradation is highly impacted by its operation; thus, Figure 8 presents a comparison of working hours (left) and toggles (right) between all three schedulers. Interestingly, RBC achieves a 7.59% reduction in working hours and a 3.48% reduction in toggling compared to the MPC. This could happen since the RBC sets the FC to work for maximum allowed power generation, i.e., 2 kWh, while MPC also uses smaller power generation based on energy demand. Accordingly, RBC has fewer working hours and reduced toggling between on/off states. As already mentioned, all three schedulers are set to operate at a maximum of 80% of the maximum power defined by the datasheet, as working at higher power generation may accelerate the degradation of the FC. The ComEMS4Build operates the FC based on demand, therefore it also uses lower power generation (see Figures 4 and 5). Accordingly, it exhibits higher working hours and more frequent state changes compared to MPC, indeed 48.44% and 6.09%, respectively. However, the increase in working hours stems from a reduced FC load.

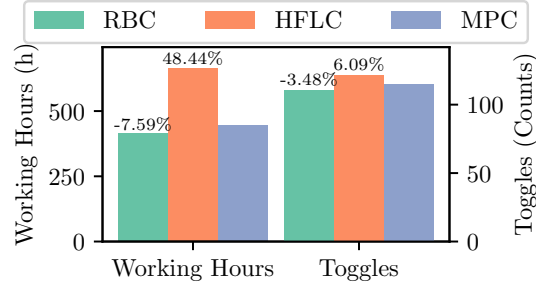


Figure 8: Working hours and toggles of the FC for the evaluation period of three months.

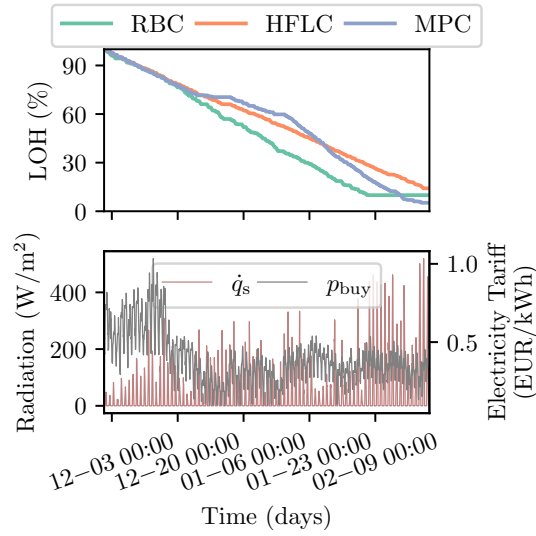


Figure 9: H_2 consumption (upper subplot) and electricity price signal and solar radiation (bottom subplot) throughout the entire evaluation period.

Figure 9 depicts the H_2 consumption over the entire period of the evaluation in the upper subplot with external signals in the bottom subplot, i.e., dynamic electricity tariff p_{buy} and the solar radiation \dot{q}_s . The MPC considers the H_2 consumption dynamically. For example, during the period from December 20 to January 6, electricity prices are lower compared to the period before December 20, indicating a more favorable state in the main grid. During this period, MPC buys more energy from the grid, reserving the H_2 supply for later use. After January 23, when electricity tariffs increase slightly, it becomes optimal to consume H_2 rather than buy electricity when high price peaks occur. The ComEMS4Build uses the H_2 mostly linearly with no external impact of electricity tariffs p_{buy} or solar radiation \dot{q}_s , keeping at the end of the simulation most H_2 supply in the storage. This relatively equal distribution of the H_2 consumption comes from the fact that ComEMS4Build considers only the EDF electricity price signal \hat{p}_{buy} , i.e., the relative placement of the current electricity price p_{buy} compared to a day-ahead grid state. In that sense, ComEMS4Build uses the H_2 when the situation in the main grid is mostly unfavorable during that day. On the other hand, MPC considers additionally the absolute price signal, making the decision based on the current price p_{buy} but also the day-ahead price distribution. Furthermore, after 12-week evaluation period, LOH left in the storage by RBC, ComEMS4Build and MPC are 9.94%, 14.14%, 5.21% respectively. Potential savings from the rest of the H_2 would be 68.68 €, 97.75 € and 36.04 €, when multiplying the rest of the H_2 by average electricity price signal within 12-weeks evaluation period $p_{buy,avg} = 0.39 \text{ €/kWh}$. This would bring the RBC and ComEMS4Build closer to the MPC in terms of reduced electricity costs (see the middle subplot in Figure 6). However, it would increase the FC operation time. Moreover, it could impact the reimbursement costs of the RBC as it sells residual energy coming from FC when

necessary.

4.4. Grid Utilization

The grid utilization is illustrated in Figure 10 as the weekly energy purchased and sold. As the selling price is constant, the sold energy (bottom plot) is proportional to the reimbursement costs (see third subplot in Figure 6). This does not pertain to purchased energy (upper subplot), as the electricity tariff is a dynamic signal. According to the reimbursement costs, MPC has a zero median of weekly sold power, while ComEMS4Build and RBC have 8.34 kWh and 35.81 kWh, respectively. Comparing the reimbursement costs with sold energy, RBC gets only 2.18€ more weekly than ComEMS4Build, but sells 27.47 kWh more energy than ComEMS4Build, comparing the median values. Furthermore, the purchased energy follows a similar trend to electricity costs but with the following medians: MPC 70.19 kWh, ComEMS4Build 92.89 kWh, and RBC 145.71 kWh. MPC has an outlier in week three, when external conditions are unfavorable, purchases 164.92 kWh of energy. In the same week, ComEMS4Build has slightly bigger consumption of 180.11 kWh, while RBC purchases 191.75 kWh.

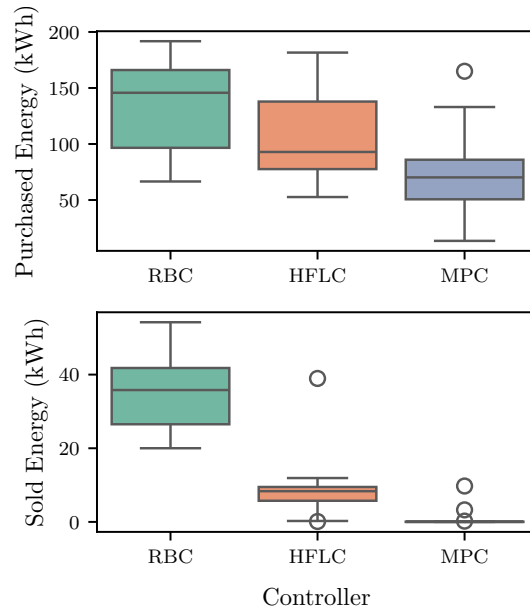


Figure 10: Weekly grid utilization for all three controllers.

4.5. Heat recovery from FC

Figure 11 shows the weekly heat recovery from FC for all three schedulers, evaluated when the FC efficiency is 75% and when it reaches 90%, shown as bars with transparency. Additionally, the DHW demand, including the DHW storage losses, is depicted for each week. It can be concluded that when FC efficiency is 75%, it can not cover the whole weekly DHW demand. Examining the RBC, with 90% of the FC systems' efficiency, can sometimes meet the weekly demand. This occurs in weeks 4, 6, 7 and 8. As the EDF prices in these weeks are in the highest quartile for an extended period, i.e., the dynamic prices have flattened peaks, the RBC, as designed, uses the HESS to cover the electrical demand and generates heat as a by-product. However, the RBC uses up all the H_2 two weeks before the end of the evaluation period because it has no input on the quantity of H_2 available.

The MPC heat generation, for example, in weeks 5 and 12, is only 11.54 kWh and 14.43 kWh, respectively, when FC efficiency is 75% and 24.79 kWh and 27.89 kWh, respectively, when FC efficiency is 90%. This happens as the electricity prices in these weeks are reaching values under 0.2 €/kWh, where MPC finds it more optimal to use the main grid rather than the FC. Accordingly, it prioritizes purchased power over the heat recovered from FC, even though the recovered heat also directly impacts electricity costs as it reduces the work of the HP. In only two weeks,

8 and 9, the MPC satisfies the entire DHW demand with the heat recovered from the FC and only when the FC system's efficiency is 90%. In these cases, the heat recovered is 68.17 kWh and 61.97kWh while the respective DHW demands are 62.56 kWh and 58.62 kWh. Those two weeks are characterized by high electricity price discrepancy (0.1-0.54 €/kWh) where MPC uses the grid only when the prices are lowest, for the rest it uses the HESS system, achieving to cover the DHW demand with recovered heat from FC. The ComEMS4Build usually has the lowest heat recovered from FC as it uses the FC for lower power generation than 2 kW (see Figures 4-5). Thus, FC exhibits higher electrical efficiency when generating less power, i.e., it consumes less H₂. Consequently, the heat recovered is lower for lower H₂ consumption.

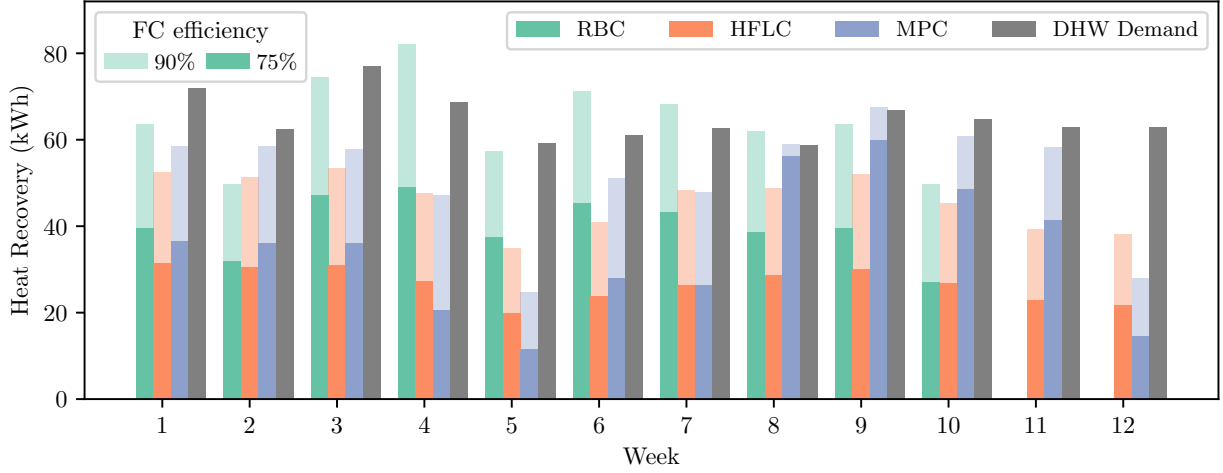


Figure 11: Weekly heat recovery from FC with 75% and 90% of systems efficiency.

5. Discussion

The results show that ComEMS4Build is more advantageous than RBC in terms of occupant-oriented indicators. It does not exhibit discomfort in 10 out of 12 weeks. RBC is acting as hysteresis, heating up until $T_{air,max} = 24^{\circ}C$ and cooling down to $T_{air,min} = 21^{\circ}C$ with sometimes slight overshoots (see the left subplot in Figure 6). Compared to RBC, ComEMS4Build exhibits significantly more stable temperature changes without frequent temperature fluctuations between $T_{air,min}$ and $T_{air,max}$ (see Figure 4). The ComEMS4Build increases the indoor air temperature, T_{air} , when either the grid is in a favorable state or there is high PV generation (see Figure 5). This provides an opportunity to store thermal energy in the TBM, shifting the load from peak to off-peak hours. The RBC sells significantly more energy to the grid than ComEMS4Build and MPC, as it operates the FC at its maximum permissible power. After satisfying the demand, it charges the BESS and sells the residual energy. However, MPC does not find it optimal to sell the energy as the reimbursement price is too low, but rather to retain it within the building. When it comes to the operation of the FC, RBC achieves a reduction in working hours and toggling compared to MPC. This is advantageous as both impact the FC degradation. However, ComEMS4Build increases the toggling slightly and working hours for almost half compared to MPC. This means that ComEMS4Build operates the FC to work longer with a smaller load. This feature highlights the increase in electrical efficiency of the FC. In this context, the electrical efficiency of the FC increases with a decrease in the power generated by FC. When it comes to the heat recovered, none of the schedulers manage to cover the DHW demand with only heat from FC in a case when FC's system efficiency in cogeneration mode is $\eta_{FC} = 75\%$. On the other hand, a higher efficiency, $\eta_{FC} = 90\%$, provides RBC with the opportunity to meet demand solely with recovered heat. However, as already discussed, the RBC uses significantly more H₂ at the beginning of the evaluation period and thus empties the H₂ storage to LOH_{min} before the end of the evaluation period (see Figure 9). ComEMS4Build usually has less heat recovered than MPC, as it operates on lower FC loads, which result in higher electrical efficiencies but produce less heat. Figure 12 summarizes the qualitative comparison of the features and the performance of all three controllers.

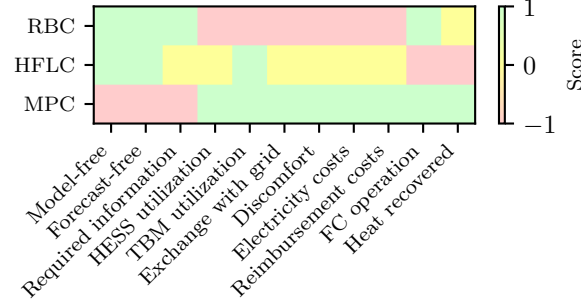


Figure 12: Qualitative comparison of the features and performance of all three controllers. Red or "-1" in score presents the bad performance (or feature), yellow or "zero" average performance (or feature), and green or "1" is good performance (or feature).

Although MPC can achieve the cost-optimal behavior, it is worth mentioning that it requires a forecasting model as well as the forecasting demand profiles, which makes MPC a fragile solution, as some profiles are highly stochastic, e.g., the DHW demand profile. The overall number of inputs required by MPC is the highest. Besides the sensors that need to be installed, the MPC would further require the training and retraining of the models, such as a thermal building model (Section 2.1.6). In this sense, the ComEMS4Build is more favorable, as it does not require either forecasting models or profiles. However, it can always offer a "good-enough" solution. The ComEMS4Build reduces the number of necessary inputs for three compared to the MPC, not requiring the forecasting models, profiles, and ambient temperature T_{amb} . The RBC further reduces the number of required inputs for four compared to ComEMS4Build as it does not require the inputs about future temperature bounds $T_{air,min}$ and $T_{air,max}$ defined by occupants, solar radiation \dot{q}_s , former state of the FC and daily permissible amount of H_2 for utilization.

6. Conclusions

Distributed Energy Resources (DER) within residential buildings are gaining attention as they can contribute to alleviating the main grid's peak demands. Battery Energy Storage System (BESS) achieve flexibility as a short-term storage solution, facilitating load shifting on a daily and up to weekly timescales. For capturing energy seasonally, one possible solution could be to convert renewable energy into H_2 for later use during periods of higher demand. In the present paper, we introduce a novel scheduling algorithm, a Comfort-Oriented Energy Management System for Residential Buildings (ComEMS4Build), for managing Hybrid Energy Storage System (HESS), which consists of a BESS and H_2 storage, coupled with HP and renewable generation from Photovoltaics (PV). In addition to that, the ComEMS4Build incorporates the thermal comfort of occupants in the scheduling algorithm and thermal storage, along with TBM, as an auxiliary flexibility medium. The scheduler is compared with Model Predictive Control (MPC), which serves as an optimal benchmark with a perfect forecast. The present study further compares ComEMS4Build with the Rule-Based Control (RBC) scheduler, developed as a simplified ComEMS4Build and used as a lower benchmark. As ComEMS4Build does not require much more inputs than RBC and operates as a model- and forecast-free scheduler, it improves occupant-oriented indicators, HESS utilization, and scheduling of energy exchanged with the main grid. As the ComEMS4Build scheduler does not rely on forecasting models or profiles and requires fewer inputs for operation, it can be a good candidate for real-world deployment. However, it increases the number of toggling and working hours of the FC, compared to both MPC and RBC, as it works with lower FC loads and higher FC electrical efficiencies. Moreover, none of the scheduling algorithms can meet the DHW demand for the entire evaluation period using only the heat recovered from FC.

Several avenues for future research are worth investigating. The scenario should be taken into account to evaluate H_2 generation in the building during the South-West German summer period, when demand for residential cooling exists. A sensitivity parameter analysis should be performed on the components within the setup to analyze their impact on the comprehensive system. Additionally, the economic analysis could be undertaken to assess at which level (single or more buildings or microgrid level) this setup would be economically beneficial and what component

dimensions would be optimal. Furthermore, more detailed models could be utilized for evaluation in a co-simulation environment, where MPC does not have a perfect forecast.

Acknowledgments

We acknowledge the financial support of the Helmholtz Association of German Research Centres (HGF) within the framework of the Program-Oriented Funding POF IV in the program Energy Systems Design (ESD, project numbers 37.12.01, 37.12.02 and 37.12.03).

Declaration of generative AI and AI-assisted technologies in the writing process

During the preparation of this work, the authors used ChatGPT in order to improve the presentation of the manuscript. After using this tool, the authors reviewed and edited the content and take full responsibility for the content of the publication.

References

- [1] G. Shahgholian, A brief review on microgrids: Operation, applications, modeling, and control, *International Transactions on Electrical Energy Systems* 31 (6) (2021) e12885. doi:10.1002/2050-7038.12885.
- [2] P. E. Dodds, I. Staffell, A. D. Hawkes, F. Li, P. Grünewald, W. McDowall, P. Ekins, Hydrogen and fuel cell technologies for heating: A review, *International Journal of Hydrogen Energy* 40 (5) (2015) 2065–2083. doi:10.1016/j.ijhydene.2014.11.059.
- [3] G. Cau, D. Cocco, M. Petrollese, S. K. Kær, C. Milan, Energy management strategy based on short-term generation scheduling for a renewable microgrid using a hydrogen storage system, *Energy Conversion and Management* 87 (2014) 820–831. doi:10.1016/j.enconman.2014.07.078.
- [4] G. De Carne, S. M. Maroufi, H. Beiranvand, V. De Angelis, S. D'Arco, V. Gevorgian, S. Waczowicz, B. Mather, M. Liserre, V. Hagenmeyer, The role of energy storage systems for a secure energy supply: A comprehensive review of system needs and technology solutions, *Electric Power Systems Research* 236 (2024) 110963. doi:https://doi.org/10.1016/j.epsr.2024.110963.
- [5] Y. Zhang, P. E. Campana, A. Lundblad, J. Yan, Comparative study of hydrogen storage and battery storage in grid connected photovoltaic system: Storage sizing and rule-based operation, *Applied Energy* 201 (2017) 397–411. doi:10.1016/j.apenergy.2017.03.123.
- [6] L. Esposito, M. Van Der Wiel, C. Acar, Hydrogen storage solutions for residential heating: A thermodynamic and economic analysis with scale-up potential, *International Journal of Hydrogen Energy* 79 (2024) 579–593. doi:10.1016/j.ijhydene.2024.06.279.
- [7] A. J. G. Mena, A. Bouakkaz, J. M. A. Pereira, L. S. Guerrero, M. d. l. L. M. Rodriguez, Collective hydrogen stand-alone renewable energy systems for buildings in Spain. towards the self-sufficiency, *International Journal of Hydrogen Energy* 72 (2024) 1274–1286. doi:10.1016/j.ijhydene.2024.05.438.
- [8] G. Naumann, E. Schropp, N. Stegmann, M. C. Möller, M. Gaderer, Environmental performance of a hybrid solar-hydrogen energy system for buildings, *International Journal of Hydrogen Energy* 49 (2024) 1185–1199. doi:10.1016/j.ijhydene.2023.07.208.
- [9] H. R. Ellamla, I. Staffell, P. Bujlo, B. G. Pollet, S. Pasupathi, Current status of fuel cell based combined heat and power systems for residential sector, *Journal of Power Sources* 293 (2015) 312–328. doi:10.1016/j.jpowsour.2015.05.050.
- [10] H. Q. Nguyen, B. Shabani, Proton exchange membrane fuel cells heat recovery opportunities for combined heating/cooling and power applications, *Energy Conversion and Management* 204 (2020). doi:10.1016/j.enconman.2019.112328.
- [11] T. Liang, X. Zhang, J. Tan, Y. Jing, L. Liangnian, Deep reinforcement learning-based optimal scheduling of integrated energy systems for electricity, heat, and hydrogen storage, *Electric Power Systems Research* 233 (2024) 110480. doi:10.1016/j.epsr.2024.110480.
- [12] S. Wang, L. Kong, C. Liu, G. Cai, MPC-based energy optimization and regulation for zero-carbon energy supply building, *International Journal of Hydrogen Energy* 82 (2024) 1196–1210. doi:10.1016/j.ijhydene.2024.07.397.
- [13] R. Shyni, M. Kowsalya, Hess-based microgrid control techniques empowered by artificial intelligence: A systematic review of grid-connected and standalone systems, *Journal of Energy Storage* 84 (2024) 111012. doi:10.1016/j.est.2024.111012.
- [14] A. Kaabinejadian, A. Pozarlik, C. Acar, A systematic review of predictive, optimization, and smart control strategies for hydrogen-based building heating systems, *Applied Energy* 379 (2025) 124994. doi:10.1016/j.apenergy.2024.124994.
- [15] Y. Yang, Z. Wu, J. Yao, T. Guo, F. Yang, Z. Zhang, J. Ren, L. Jiang, B. Li, An overview of application-oriented multifunctional large-scale stationary battery and hydrogen hybrid energy storage system, *Energy Reviews* 3 (2) (2024) 100068. doi:https://doi.org/10.1016/j.enrev.2024.100068.
- [16] J. Go, J. Byun, K. Orehounig, Y. Heo, Battery-H₂ storage system for self-sufficiency in residential buildings under different electric heating system scenarios, *Applied Energy* 337 (2023) 120742. doi:10.1016/j.apenergy.2023.120742.
- [17] T. S. Le, T. N. Nguyen, D.-K. Bui, T. D. Ngo, Optimal sizing of renewable energy storage: A techno-economic analysis of hydrogen, battery and hybrid systems considering degradation and seasonal storage, *Applied Energy* 336 (2023) 120817. doi:https://doi.org/10.1016/j.apenergy.2023.120817.
- [18] M. A. Giovanniello, X.-Y. Wu, Hybrid lithium-ion battery and hydrogen energy storage systems for a wind-supplied microgrid, *Applied Energy* 345 (2023) 121311. doi:https://doi.org/10.1016/j.apenergy.2023.121311.
- [19] A. Çiçek, A novel resilience-oriented energy management strategy for hydrogen-based green buildings, *Journal of Cleaner Production* 470 (2024) 143297. doi:10.1016/j.jclepro.2024.143297.

- [20] J. Li, W. Zou, Q. Yang, H. Bao, Towards net-zero smart system: An power synergy management approach of hydrogen and battery hybrid system with hydrogen safety consideration, *Energy Conversion and Management* 263 (2022) 115717. doi:10.1016/j.enconman.2022.115717.
- [21] K. Ou, W.-W. Yuan, Y.-B. Kim, Development of optimal energy management for a residential fuel cell hybrid power system with heat recovery, *Energy* 219 (2021) 119499. doi:10.1016/j.energy.2020.119499.
- [22] M. Gandiglio, A. Lanzini, M. Santarelli, P. Leone, Design and optimization of a proton exchange membrane fuel cell CHP system for residential use, *Energy and Buildings* 69 (2014) 381–393. doi:10.1016/j.enbuild.2013.11.022.
- [23] S.-D. Oh, K.-Y. Kim, S.-B. Oh, H.-Y. Kwak, Optimal operation of a 1-kW PEMFC-based CHP system for residential applications, *Applied Energy* 95 (2012) 93–101. doi:10.1016/j.apenergy.2012.02.019.
- [24] D. Mariano-Hernández, L. Hernández-Callejo, A. Zorita-Lamadrid, O. Duque-Pérez, F. Santos García, A review of strategies for building energy management system: Model predictive control, demand side management, optimization, and fault detect & diagnosis, *Journal of Building Engineering* 33 (2021) 101692. doi:https://doi.org/10.1016/j.jobbe.2020.101692.
- [25] F. Vivas, F. Segura, J. Andújar, Fuzzy logic-based energy management system for grid-connected residential DC microgrids with multi-stack fuel cell systems: A multi-objective approach, *Sustainable Energy, Grids and Networks* 32 (2022). doi:10.1016/j.segan.2022.100909.
- [26] D. C. Šanić, F. Barbir, Stand-alone micro-trigeneration system coupling electrolyzer, fuel cell, and heat pump with renewables, *International Journal of Hydrogen Energy* 47 (82) (2022) 35068–35080. doi:10.1016/j.ijhydene.2022.08.090.
- [27] J. Sievers, P. Henrich, M. Beichter, R. Mikut, V. Hagenmeyer, T. Blank, F. Simon, Federated reinforcement learning for sustainable and cost-efficient energy management, *Energy and AI* 21 (2025) 100521. doi:https://doi.org/10.1016/j.egyai.2025.100521.
- [28] M. Ławryńczuk, Computationally efficient model predictive control algorithms, A Neural Network Approach, *Studies in Systems, Decision and Control* 3 (2014). doi:10.1007/978-3-319-04229-9.
- [29] D. Q. Mayne, Model predictive control: Recent developments and future promise, *Automatica* 50 (12) (2014) 2967–2986. doi:https://doi.org/10.1016/j.automatica.2014.10.128.
- [30] S. M. Maroufi, S. Karrari, K. Rajashekaraiah, G. De Carne, Power management of hybrid flywheel-battery energy storage systems considering the state of charge and power ramp rate, *IEEE Transactions on Power Electronics* 40 (7) (2025) 9944–9956. doi:10.1109/TPEL.2025.3546013.
- [31] A. R. Boynuegri, B. Tekgun, Real-time energy management in an off-grid smart home: Flexible demand side control with electric vehicle and green hydrogen production, *International Journal of Hydrogen Energy* 48 (60) (2023) 23146–23155. doi:10.1016/j.ijhydene.2023.01.239.
- [32] K. Knosala, L. Langenberg, N. Pflugradt, P. Stenzel, L. Kotzur, D. Stolten, The role of hydrogen in German residential buildings, *Energy and Buildings* 276 (2022) 112480. doi:10.1016/j.enbuild.2022.112480.
- [33] T. S. Andrade, S. K. Nalini Ramakrishna, T. Thiringer, Integrating a fuel cell with a heat pump: An energy-saving system for residential housing, *Energy Conversion and Management* 326 (Feb. 2025). doi:10.1016/j.enconman.2025.119509.
- [34] M. J. M. Al Essa, Home energy management of thermostatically controlled loads and photovoltaic-battery systems, *Energy* 176 (2019) 742–752. doi:10.1016/j.energy.2019.04.041.
- [35] I. Hazyuk, C. Ghiaus, D. Penhouet, Optimal temperature control of intermittently heated buildings using model predictive control: Part i-building modeling, *Building and Environment* 51 (2012) 379–387. doi:10.1016/j.buildenv.2011.11.009.
- [36] A. Rouhani, H. Kord, M. Mehrabi, A comprehensive method for optimum sizing of hybrid energy systems using intelligence evolutionary algorithms, *Indian Journal of Science and Technology* 6 (6) (2013) 4702–4712.
- [37] M. S. Javadi, M. Gough, M. Lotfi, A. E. Nezhad, S. F. Santos, J. P. Catalão, Optimal self-scheduling of home energy management system in the presence of photovoltaic power generation and batteries, *Energy* 210 (2020) 118568. doi:10.1016/j.energy.2020.118568.
- [38] I. Firtina-Ertis, C. Acar, E. Erturk, Optimal sizing design of an isolated stand-alone hybrid wind-hydrogen system for a zero-energy house, *Applied Energy* 274 (2020) 115244. doi:10.1016/j.apenergy.2020.115244.
- [39] R. Lacko, B. Drobnič, M. Sekavčnik, M. Mori, Hydrogen energy system with renewables for isolated households: The optimal system design, numerical analysis and experimental evaluation, *Energy and Buildings* 80 (2014) 106–113. doi:10.1016/j.enbuild.2014.04.009.
- [40] C. Acar, E. Erturk, I. Firtina-Ertis, Performance analysis of a stand-alone integrated solar hydrogen energy system for zero energy buildings, *International Journal of Hydrogen Energy* 48 (5) (2023) 1664–1684. doi:10.1016/j.ijhydene.2022.10.051.
- [41] T. Dengiz, P. Jochem, W. Fichtner, Demand response with heuristic control strategies for modulating heat pumps, *Applied Energy* 238 (2019) 1346–1360. doi:10.1016/j.apenergy.2018.12.008.
- [42] F. Langner, W. Wang, M. Frahm, V. Hagenmeyer, Model predictive control of distributed energy resources in residential buildings considering forecast uncertainties, *Energy and Buildings* 303 (2024) 113753. doi:10.1016/j.enbuild.2023.113753.
- [43] aWATTar GmbH, Electricity tariff with hourly price adjustment, Last accessed: June 2, 2025. URL <https://www.awattar.at/>
- [44] Gurobi Optimization LLC, Gurobi, Last accessed: October 10, 2025. URL <https://docs.gurobi.com/current/>
- [45] University of Kassel, DHWcalc, Last accessed: June 1, 2025. URL <https://www.uni-kassel.de/maschinenbau/en/institute/thermische-energietechnik/fachgebiete/solar-und-anlagentechnik/downloads>
- [46] N. Pflugradt, P. Stenzel, L. Kotzur, D. Stolten, Loadprofilegenerator: An agent-based behavior simulation for generating residential load profiles, *Journal of Open Source Software* 7 (71) (2022) 3574. doi:10.21105/joss.03574.
- [47] Bundesnetzagentur, Remuneration for electricity fed into the grid, Last accessed: June 12, 2025. URL https://www.bundesnetzagentur.de/DE/Fachthemen/ElektrizitaetundGas/ErneuerbareEnergien/EEG_Foerderung/start.html
- [48] DWD, German Weather Service, Last accessed: June 2, 2025. URL <https://www.wetterdienst.de/>

- [49] T. Ueno, A. Meier, A method to generate heating and cooling schedules based on data from connected thermostats, *Energy and Buildings* 228 (2020) 110423. doi:10.1016/j.enbuild.2020.110423.
- [50] F. Wiegel, J. Wachter, M. Kyesswa, R. Mikut, S. Waczowicz, V. Hagenmeyer, Smart energy system control laboratory—a fully-automated and user-oriented research infrastructure for controlling and operating smart energy systems, *at-Automatisierungstechnik* 70 (12) (2022) 1116–1133. doi:10.1515/auto-2022-0018.
- [51] Viessmann Community, Planungshandbuch Wärmepumpen, Last accessed: July 2, 2024.
URL https://community.viessmann.de/viessmann/attachments/viessmann/customers-heatpump-hybrid/16971/1/pr-planungshandbuch_waermepumpen.pdf
- [52] German Environment Agency, Ökodesign-Richtlinie und Energieverbrauchskennzeichnung1, Last accessed: June 1, 2025.
URL https://www.umweltbundesamt.de/sites/default/files/medien/376/dokumente/oekodesignrichtlinie_und_energieverbrauchskennzeichnung_warmwasserbereiter.pdf
- [53] Swiss Tech, Fresh Water Stations, Last accessed: July 28, 2025.
URL <https://merkblatt.suissetec.ch/de-CH/ALLE222/file/ALLE222.pdf>
- [54] LG, Therma V Monobloc HM051M U43, Last accessed: June 2, 2025.
URL [https://www.lg.com/de/business/download/airsolution/R32_Monobloc_Silent%20Monobloc_Leaflet_DE_20210208\[20210208_235539521\].pdf?srs1tid=AfmB0orN1n8UF-Pyi6a6GJsuqSPikGJox9LpR2DKpP0Ssy0kF9zRMEZC](https://www.lg.com/de/business/download/airsolution/R32_Monobloc_Silent%20Monobloc_Leaflet_DE_20210208[20210208_235539521].pdf?srs1tid=AfmB0orN1n8UF-Pyi6a6GJsuqSPikGJox9LpR2DKpP0Ssy0kF9zRMEZC)
- [55] Horizon Fuel Cell Europe, s.r.o, Horizon Educational, Last accessed June 20, 2025.
URL <https://www.horizoneducational.com/>
- [56] T. Fletcher, R. Thring, M. Watkinson, An Energy Management Strategy to concurrently optimise fuel consumption & PEM fuel cell lifetime in a hybrid vehicle, *International Journal of Hydrogen Energy* 41 (46) (2016) 21503–21515. doi:10.1016/j.ijhydene.2016.08.157.
- [57] R. Stropnik, N. Mlakar, A. Lotrič, M. Sekavčnik, M. Mori, The influence of degradation effects in proton exchange membrane fuel cells on life cycle assessment modelling and environmental impact indicators, *International Journal of Hydrogen Energy* 47 (57) (2022) 24223–24241. doi:10.1016/j.ijhydene.2022.04.011.
- [58] NKON B.V., PYLONTECH US5000-1C 48V 4.8kWh Home Battery, Last accessed: August 8, 2025.
URL <https://www.nkon.nl/en/pylontech-us-5000-48-v.html>
- [59] The Fuel Cell Store, Hydrogen Fuel Cell Power Generator, Last accessed: August 8, 2025.
URL <https://www.fuelcellstore.com/g-hfcs-2kw25v-1kw-hydrogen-fuel-cell-power-generator>
- [60] M. Mork, A. Xhonneux, D. Müller, Nonlinear distributed model predictive control for multi-zone building energy systems, *Energy and Buildings* 264 (2022) 112066.
- [61] I. H. Altas, et al., Fuzzy logic control in energy systems with design applications in matlab/simulink, *Tech. rep.*, IET (2017). doi:10.1049/PBP0091E.

Appendix A. ComEMS4Build design

The Mamdani fuzzy inference system [61] is utilized for the design of the FLCs. For the rule combination, the minimum function operator is chosen, while the fuzzy conclusion is derived by the maximum operator, and the defuzzification method is the Center of Gravity (CoG).

Figure A.13 illustrates the inputs and outputs of the ComEMS4Build scheduler. First two plots in the first row have same legend, where "empty" and "full" refer to SOC, LOH and ΔLOH while "low" and "high" refer to $\chi_{\text{SH}}, \chi_{\text{DHW}}, \hat{p}_{\text{buy}}$ and \dot{q}_s . The third subplot in the first row depicts the membership function of the binary variable $s_{\text{on/off}}$. The fourth subplot in the first row and the first plot in the second row depict membership functions of loads ΔP and ΔP_{new} normalized on the scale 10 kW. To determine membership functions, specific system values are used. For the peak of the "medium negative" membership function ΔP , the load that can be covered only by FC is chosen. For the peak of "big negative" membership function ΔP , the load that both can cover by FC and BESS is selected. The same applies to ΔP_{new} , where the "medium positive" and the "medium negative" peaks refer to half of the batteries' charging and discharging power, respectively. Identically, the "big positive" and the "big negative" ΔP_{new} load peaks refer to the full batteries' charging and discharging power, respectively. The latter three subplots in the Figure A.13 illustrate the membership functions of control signals: α_{HP} , α_{B} and α_{FC} . Note that the first three subplots in the second row have the same legend where "zero" refers to the ΔP_{new} and α_{HP} , and "off" to the α_{B} membership function.

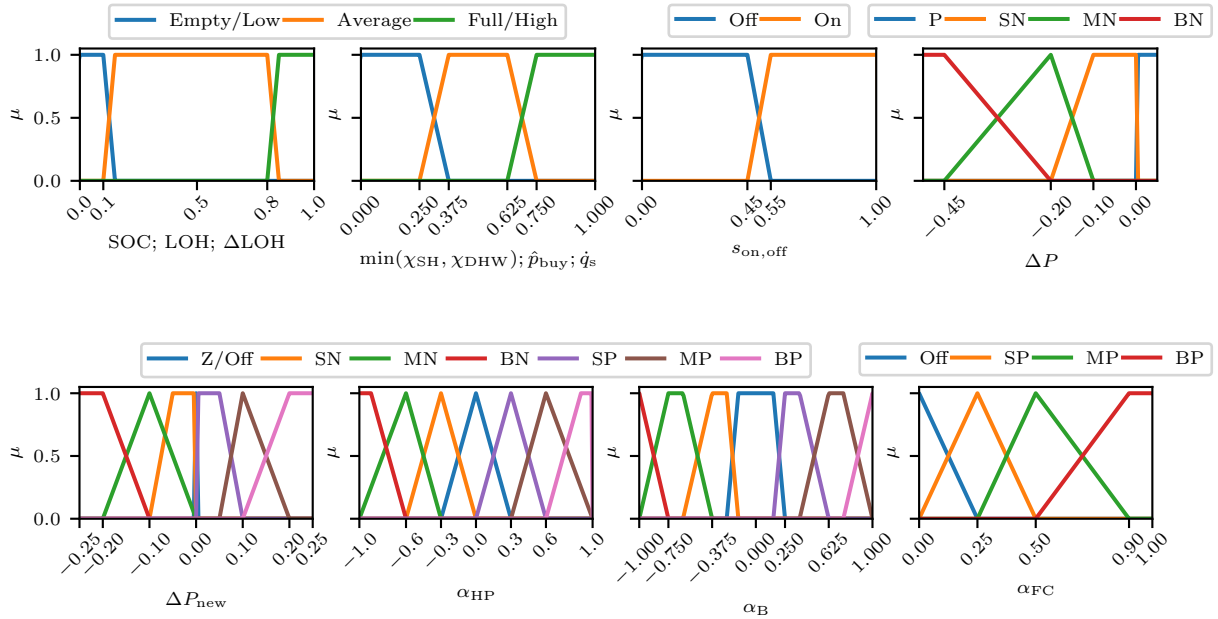


Figure A.13: Membership functions for the inputs and control signals of the ComEMS4Build scheduler. Note that the first two subplots in the first row and the first three subplots in the second row have the common labels.

Table A.4 presents a section of the FLC_{flex} rules. For example, suppose the state in the HESS is not favorable, SOC and LOH are indicating "empty", and solar radiation \dot{q}_s is "low", and the \hat{p}_{buy} shows the lowest electricity prices in timestep k compared to day-ahead prices, the output α_{B} will be "big positive" (see first rule in Table A.4). However, if the EDF electricity prices \hat{p}_{buy} are the highest at the time step k the FLC_{flex} will work in saving mode with an output $\alpha_{\text{HP}} = \text{"Z"}$ indicating "zero" (see second rule in Table A.4). Furthermore, if the EDF electricity prices \hat{p}_{buy} are "high" but the solar radiation \dot{q}_s is also "high" the scheduler will operate the HP to store additional energy in TBM, by increasing the HP electrical demand (see third rule in Table A.4). The seventh rule illustrates the following conditions: the thermal state in the building is favorable, e.g., $\min(\chi_{\text{SH}}, \chi_{\text{DHW}})$ is "high", the H_2 storage is "empty", SOC is "average", \hat{p}_{buy} is "high" and \dot{q}_s is "low". As a result, the scheduler will work in saving mode, giving the

output α_{HP} = "big negative". The control output α_{HP} presents the increment or decrement of the HP modulation factor η_{HP} from the previous timestep:

$$\eta_{HP}[k] = \alpha_{HP} \cdot \eta_{HP}[k - 1] \quad (A.1)$$

Table A.4: The rules snapshot for FLC_{flex}. The abbreviations in the table are as follows: BP - big positive; Z - zero; SP - small positive; BN - big negative.

Rules	$\min(\chi_{SH}, \chi_{DHW})$	LOH	SOC	\hat{p}_{buy}	\dot{q}_s	α_{HP}
1.	Low	Empty	Empty	Low	Low	BP
2.	Low	Empty	Empty	High	Low	Z
3.	Low	Empty	Empty	High	High	BP
4.	Low	Average	Average	Average	Average	BP
5.	Low	Full	Full	High	Low	BP
6.	Average	Empty	Empty	Average	High	SP
7.	High	Empty	Average	High	Low	BN

Table A.5: The rules snapshot for FLC_{FC}. The abbreviations in the table are as follows: MP - medium positive; BP - big positive; SN - small negative; MN - medium negative; BN - big negative.

Rules	ΔP	ΔLOH	SOC	\hat{p}_{buy}	$s_{on,off}$	α_{FC}
1.	SN	Empty	Full	High	Off	Off
2.	SN	Average	Empty	Average	Off	Off
3.	SN	Average	Empty	Average	On	MP
4.	MN	Average	Empty	Low	Off	Off
5.	MN	Average	Empty	High	Off	BP
6.	MN	Full	Empty	High	Off	BP
7.	BN	Average	Empty	Average	On	BP

Table A.5 depicts part of the rule base for FC operation. For example, the second and third rules depict the situation where the operation of the FC depends on the previous state of the FC $s_{on/off}[k - 1]$. The load ΔP is "small negative", the permissible amount of the H₂ for daily usage ΔLOH is "average". At the same time, the BESS is empty and the EDF electricity price \hat{p}_{buy} is "average". In this case, if the FC was in operation in time step $k - 1$, the output signal will be "medium positive" (the third rule in Table A.5), but if the FC was not working in previous time step $k - 1$, it will stay "off" (the second rule in Table A.5). Furthermore, if the EDF electricity price \hat{p}_{buy} is "high" but there is "average" or "full" daily permissible amount of H₂ to use ΔLOH , the FC will be switched on with α_{FC} = "big positive" (see fifth and sixth rules). The control output α_{FC} directly impacts the power generated from H₂, as it is multiplied by the maximal FC power $P_{el,FC,max}$ and security factor ζ :

$$P_{el,FC} = \alpha_{FC} \cdot P_{el,FC,max} \cdot \zeta \quad (A.2)$$

Battery management FLC_B depends on the residual load that needs to be covered ΔP_{new} , SOC, and \hat{p}_{buy} , Table A.6. Suppose the SOC is "empty" and \hat{p}_{buy} is "low" and the residual load indicates "small negative" load. The output of the scheduler α_B will define the battery charging as "big positive", as the purchasing price is currently favorable, and the residual load ΔP_{new} will be purchased from the main grid (see first rule):

$$P_{buy} = \Delta P_{new} + \alpha_B \cdot P_{ch,max} \quad (A.3)$$

On the other hand, if the SOC is "average" and the \hat{p}_{buy} is "high", the battery will cover the residual load, and if necessary, the rest will be purchased from the grid (see forth and sixth rule). This is defined as follows:

$$P_d = \alpha_B \cdot \Delta P_{new} \quad (A.4)$$

$$P_{buy} = (1 - \alpha_B) \cdot \Delta P_{new} \quad (A.5)$$

Table A.6: The rules snapshot for FLC_B . The abbreviations in the table are as follows: SN - small negative; MN - medium negative; BN - big negative; MP - medium positive; BP - big positive.

Rules	ΔP_{new}	SOC	\hat{p}_{buy}	α_B
1.	SN	Empty	Low	BP
2.	SN	Empty	High	Off
3.	SN	Average	Low	MP
4.	MN	Average	High	MN
5.	BN	Average	Average	MN
6.	BN	Average	High	BN
7.	MP	Empty	Low	BP

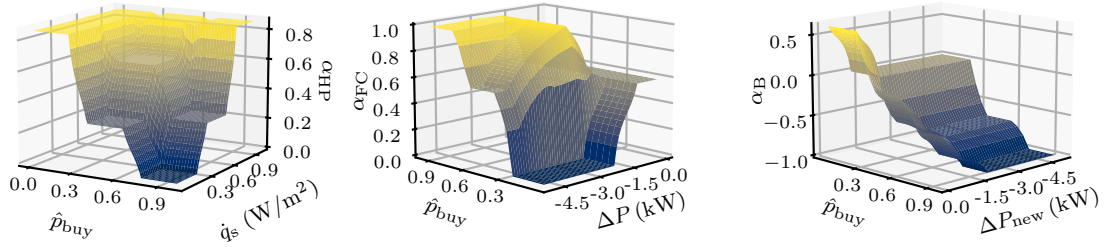


Figure A.14: Example of the ComEMS4Build input-output mapping for FLC_{flex} (left) when HESS states are $\text{SOC}[k-1] = 10\%$ and $\text{LOH}[k-1] = 10\%$. In the middle is FLC_{FC} under the condition of $\text{SOC}[k-1] = 20\%$ and $\Delta\text{LOH}[k-1] = 80\%$ while prices and load are varying. The right subplot depicts the FLC_B for $\text{SOC}[k-1] = 50\%$, while the EDF price signal and load vary.

Figure A.14 depicts the input-output mapping for FLC_{flex} (left), FLC_{FC} (middle) and FLC_B (right). In the case of FLC_{flex} , the HESS is almost empty, i.e., $\text{SOC}[k-1] = 10\%$ and $\text{LOH}[k-1] = 10\%$. FLC_{flex} is then oriented on EDF electricity prices \hat{p}_{buy} and current solar radiation \dot{q}_s . The FLC_{FC} works only when the demand exists and the permissible amount of H_2 ΔLOH to use for that day has not yet been used. The middle subfigure in Figure A.14 shows the situation when load and EDF electricity prices vary. The following inputs are kept constant: $\Delta\text{LOH}[k-1] = 80\%$, $\text{SOC}[k-1] = 20\%$, and $s_{\text{on,off}}[k-1] = \text{"on"}$. The load is depicted as negative, while excess energy has a positive value. It can be concluded that as the load and the EDF electricity price increase, the FLC_{FC} will increase the factor α_{FC} . If the load is under 1500 kW and the FC is already turned on $s_{\text{on,off}}[k-1] = \text{"on"}$, FLC_{FC} tries to cover the load alone. The right subplot in Figure A.14 shows the case of controlling the BESS by FLC_B , when $\text{SOC}[k-1] = 50\%$ and EDF electrical prices \hat{p}_{buy} and load ΔP_{new} are varying. Negative α_B factor defines the discharging state, while a positive factor defines the charging. As the low EDF prices are favorable, and when the load is smaller, the factor α_B increases. This means that the main grid will cover the load, and the energy will be purchased for charging the BESS. However, by increasing the load and electricity prices, the FLC_B tries to discharge the BESS as much as possible to cover the load.